RUHR-UNIVERSITÄT BOCHUM

Chiral fluorescence and phosphorescence

by

Chetana Badala Viswanatha

A thesis submitted in partial fulfillment for the degree of
Master of Science

in the
Faculty of Chemistry and Biochemistry
Chair for Theoretical Chemistry
Quantum Chemistry Group

September 2017

Acknowledgements

I would like to express my heartfelt gratitude to my thesis supervisor Prof. Dr. Christof Hättig. His good humoured and patient guidance have been a transformative experience. I am indebted to him for his valuable scientific ideas. My sincere thanks also go to Alireza Marefat Khah, Marius Frank and Niklas Sülzner for their help with technical questions. Many thanks to Sarah Khani, Hang Choi and Lisa Götte for making my master's work enjoyable. I am also grateful to Özlem Yönder for her presence, inputs and kind support throughout. I would also like to acknowledge Alireza for his innovative program to change torsion angles and the program for plotting CD spectrum.

Contents

Acknowledgements i

List of Figures iv

List of Tables v

Abbreviations vi

1 Introduction 1
- 1.1 The relation between CD and CPL . . . 1
- 1.2 Theoretical Approach for CD calculations . . . 2
- 1.3 Theoretical Approach for CPL calculations . . . 2
  - 1.3.1 Circularly Polarized Fluorescence (CPF) . . . 2
  - 1.3.2 Circularly Polarized Phosphorescence (CPP) . . . 2

2 Objective of the study 4

3 Theoretical Background 5
- 3.1 CD and CPL strengths in CC Response theory . . . 5
  - 3.1.1 Definitions . . . 5
    - Oscillator strength . . . 5
    - Rotator strength . . . 5
    - Dipole strength . . . 6
  - 3.1.2 Coupled Cluster theory . . . 6
  - 3.1.3 Response theory . . . 7
  - 3.1.4 Coupled Cluster Response Theory [1–3] . . . 8
  - 3.1.5 Breakdown of Perturbational ansatz[2] . . . 9
  - 3.1.6 Gauge-origin invariance . . . 9
- 3.2 Spin free formalism for CPP and Perturbation theory . . . 9
  - 3.2.1 Treatment of spin-forbidden transitions in PT . . . 9
  - 3.2.2 Spin-free formalism . . . 10
  - 3.2.3 Spin-Orbit operator . . . 11
  - 3.2.4 Matrix elements of the spin-orbit operator . . . 12
  - 3.2.5 Wigner-Eckart theorem . . . 13
  - 3.2.6 Phosphorescence . . . 13

4 Computational details 16
- 4.1 Basis sets and Methods . . . 16

Basis sets 16
Methods 16
4.2 Choice of molecules 17

5 Results and Discussion **18**
5.1 Test calculations 18
5.2 CPL 23
5.3 CPF and CPP of β,γ-enones 24
5.4 Ketones with conjugated double bonds 30
5.5 CPP in Metal-Free Chiral Aromatics 33

6 Summary **36**

A Conversion factors **38**

B Wigner-Eckart Theorem **39**
Alternative method 39

Bibliography **41**

List of Figures

4.1 Bond-line structures of β, γ-enones and conjugated ketones 17
4.2 Bond-line structures of (R)-DMBDA and (S)-DMBDA 17

5.1 The ground and first singlet excited state structures of enone **1** 24
5.2 The ground and first singlet excited state structures of enone **2** 24
5.3 The ground and first singlet excited state structures of enone **3** 25
5.4 The ground and first singlet excited state structures of enone **4** 25
5.5 Most dominant NTOs of enones **1**-**4** for the singlet excited state structures 26
5.6 The ground and first triplet excited state structures of enone **1** 27
5.7 The ground and first triplet excited state structures of enone **2** 27
5.8 The ground and first triplet excited state structures of enone **3** 27
5.9 The ground and first triplet excited state structures of enone **4** 27
5.10 Most dominant NTOs of enones **1**-**4** for the triplet excited state structures 29
5.11 The first excited triplet state structures of conjugated ketones **5**, **6** and **7** 31
5.12 Most dominant NTO for the triplet excited state structures of camphorquinone, **6** 31
5.13 The CD spectrum for singlet transitions of camphorquinone, **6** 32
5.14 The geometry-optimized structures of (S)-DMBDA 33
5.15 NTOs for the first singlet transitions of(S)-DMBDA 34
5.16 NTOs for the first and second singlet transitions of(S)-DMBDA 35
5.17 The natural transition orbitals for the circularly-polarized phosphorescence in S-DMBDA 35

List of Tables

5.1 Comparison of the RI-CC2 velocity (D^v, R^v) and length (D^l, R^l) gauge results of H_2O_2 for the DFT optimized structure. 18
5.2 Comparison between X2C-CC2 and RI-CC2 transition strengths in atomic units 19
5.3 Comparison of the RI-CC2 velocity (D^v, R^v) and length (D^l, R^l) gauge results of H_2O_2 for the CC2 optimized structure. 19
5.4 Gauge-origin dependence of rotational strengths in length gauge and velocity gauge formulations in H_2O_2 for the DFT geometry optimized ground state structure. 21
5.5 Gauge-origin dependence of rotational strengths in length gauge and velocity gauge formulations in H_2O_2 for the CC2 geometry optimized ground state structure. 22
5.6 Comparison of the rotational strengths in velocity gauge for CPF in enones 24
5.7 Vertical transition energies for CD,CPF and CPP in enones 28
5.8 Comparison of the rotational strengths in velocity gauge for CPP in enones 28
5.9 The dipole and rotational strengths in velocity gauge for singlet-triplet transitions in enone **5** 30
5.10 The rotational strengths in velocity gauge for CD,CPF and CPP transitions in diketones **6** and **7** 30
5.11 Vertical transition energies for CD,CPF and CPP in diketones **6** and **7** . . 32
5.12 Rotational strengths of S-DMBDA 35

Abbreviations

CC	**C**oupled - **C**luster
CCSD	**C**oupled -**C**luster **S**ingles and **D**oubles
CD	**C**ircular **D**ichroism
CPL	**C**ircularly **P**olarized **L**uminescence
CPF	**C**ircularly **P**olarized **F**luorescence
CPP	**C**ircularly **P**olarized **P**hosphorescence
HF	**H**artree - **F**ock
MCSCF	**M**ulti - **C**onfigurational **S**elf - **C**onsistent **F**ield
MO	**M**olecular **O**rbital
NTO	**N**atural **T**ransition **O**rbital
PT	**P**erturbational **T**heory
RI	**R**esolution - of - **I**dentity
SCF	**S**elf - **C**onsistent **F**ield
SOC	**S**pin - **O**rbit **C**oupling
TDDFT	**T**ime - **D**ependent **D**ensity **F**unctional **T**heory
WET	**W**igner -**E**ckart **T**heorem

Chapter 1

Introduction

A striking example of Circularly Polarized Luminescence (CPL) in nature was reported in 1980 [4]. The left and right lanterns of live larvae of fireflies were found to emit circularly polarized light with opposite handedness. Although CPL measurements on chiral samples dates back to 1948 [5], first principle calculations of vibrationally resolved CPL were only reported in 2010 using time-dependent density functional theory (TD-DFT)[6]. The possible use of Circular Dichroism (CD) and CPL spectra combined with theoretical calculations as a probe for conformational changes upon electronic excitation has been demonstrated since 1974[7].

1.1 The relation between CD and CPL

Circular Dichroism is the differential absorption of left and right circularly polarized light by optically-active compounds[8]. Spontaneous and induced emission of circularly polarized light is expected to occur in optically active compounds because the theoretical expressions for both light absorption and emission contain the same molecular quantities[9]. In a study by Emeis and Oosterhoff [9], circular polarisation was shown to occur both in fluorescence and phosphorescence. CPL which is the emission analogue of CD, thus measures the differential emission of left and right circularly polarized light by chiral luminescent systems[10].

1.2 Theoretical Approach for CD calculations

The difference in absorption coefficients between left and right circularly polarized light is proportional to the scalar rotatory strength for a transition from ground to excited state in randomly oriented molecules [11]. In linear response theory approach, the scalar rotatory strength can be obtained as a residue of the linear response function [12, 13]. Coupled-Cluster response calculation of natural chiroptical spectra was reported in 1999[13] using coupled-cluster singles and doubles (CCSD) model. The vertical excitation energies and structures given by the approximate Coupled-Cluster model CC2 is comparable to that of CCSD [14]. The CC2 implementation in TURBOMOLE also utilizes the RI-approximation for two electron repulsion integrals. RI-CC2 approach can be used for larger molecules because of its low computational costs [15].

1.3 Theoretical Approach for CPL calculations

1.3.1 Circularly Polarized Fluorescence (CPF)

In Fluorescence, the excited state is a singlet and the transition is spin-allowed to the singlet ground state [16]. The CPL intensity is also proportional to the rotational strength between the excited state and the ground state. The only difference in calculation is that the input structure is a geometry optimized excited state as opposed to a ground state structure in CD [11].

1.3.2 Circularly Polarized Phosphorescence (CPP)

A review article [17] on CPL asserts that TD-DFT is the widely used method for computing and interpreting CPL spectra for small to mid-sized molecules. In Phosphorescence, the excited state is a triplet and the transition is spin-forbidden to the singlet ground state [16]. For CPP, an alternative cost-effective way of computing spin-orbit coupling (SOC) matrix elements is the approximate Coupled-Cluster Singles and Doubles Method, RI-CC2. A relativistic calculation can be performed using exact two component (X2C) ansatz[18]. This is still expensive for correlated wave function methods.
The SOC effects are small for molecules with only light elements and can be treated

within the framework of perturbation theory (PT) and spin free formalism for closed shell systems using RI-CC2 [19]. An explicitly spin-coupled basis for singlet and triplet operators was used thereby avoiding spin-orbital treatment for closed shell systems. SOC-PT employed together with response theory is size extensive. Also, the spin-free formalism is cheaper than a spin-orbit based formalism by a factor of four. SOC-PT ansatz within response theory framework has also been implemented at the MCSCF [20], TDDFT [16] and CCSD [2] level for singlet-triplet transitions.

CC2 being an economic alternative to CCSD is also capable of treating larger molecules consisting only of lighter elements. The RI-CC2 implementation[19] of phosphorescence lifetimes using SOC-PT was roughly 12 times faster than a two component relativistic calculation and was calculated for a metal-free organic light emitting diode with almost 60 atoms. The accuracy of phosphorescence lifetimes for lowest triplet states in halogen hydrides did not differ by more than 50% from those obtained with X2C-CC2. However, for heavier elements like Bromine in the higher nearly degenerate states the SOC-PT-CC2 was a poor approximation because the spin-orbit corrections to the excitation energies was of the same order of magnitude as the energy differences between electronic states in a one-component calculation. The memory and disk space demands for the RI-CC2 method are reduced from $O(n^2N^2)$ in the CC2 method to , $O(N^2)$ and $O(nN^2)$ respectively [21] making RI-CC2 method capable of handling molecules 2-3 times larger than conventional CC2.

Chapter 2

Objective of the study

Molecular systems where phosphorescence contributions to emission spectra become important poses a challenge for theoretical calculations [17]. So far, a theoretical and computational protocol seems to have been developed only using TD-DFT method for certain chiral enones and diketones [16]. No experimental data has been reported for the CPP strengths of these molecules.

In this master project, an attempt was made to study the CD and CPL strengths of chiral enones and diketones from the aforementioned reference [16] using wave function based method, RI-CC2, and to extend it to a a larger metal-free chiral aromatic [22] system for which there is experimental data for room-temperature persistent CPP. This article[22] gives TD-DFT values only for spin-allowed CPL rotational strengths and not for spin-forbidden phosphorescence.

In this study, Hydrogen Peroxide was used as a test molecule to check for basis set dependency and gauge-origin invariance. Since no experimental data is available for CD rotator strengths of H_2O_2 , X2C-CC2 calculations were performed for comparison. The CPP rotator strengths were obtained using TURBOMOLE[40] package as an extension of phosphorescence lifetime code implemented in RI-CC2 [19] using SOC-PT within the framework of response theory. In order to compare the emission strengths and their relation to the excited-state structure, spin-allowed CPF calculations were performed. The CD calculations in spin-allowed and spin-forbidden transitions were also performed to study the changes in the sign of rotational strengths in absorption and emission.

Chapter 3

Theoretical Background

3.1 CD and CPL strengths in CC Response theory

3.1.1 Definitions

Oscillator strength Consider a transition between ground state $|0\rangle$ and excited state $|n\rangle$ for isotropic samples, the oscillator strength[13, 23] is given by

$$
\begin{aligned}
{}^{n}f^{v} &= \frac{2}{3\omega_n}\langle 0|\mathbf{p}|n\rangle \cdot \langle n|\mathbf{p}|0\rangle \text{ (velocity gauge)} && (3.1)\\
{}^{n}f^{r} &= \frac{2\omega_n}{3}\langle 0|\mathbf{r}|n\rangle \cdot \langle n|\mathbf{r}|0\rangle \text{ (length gauge)} && (3.2)
\end{aligned}
$$

Rotator strength The imaginary part of the dot product between electric and magnetic transition dipole moments for a transition between ψ_o and ψ_n gives the scalar rotatory strength for circular dichroism [12, 23].

$$
R(0 \rightarrow n) = Im[\langle \psi_o|\mu_{el}|\psi_n\rangle\langle \psi_o|\mu_{mag}|\psi_n\rangle] \tag{3.3}
$$

The ordinary scalar rotatory strength[13, 24] for randomly oriented samples between ground state $|0\rangle$ and excited state $|n\rangle$ is given by

$$
\begin{aligned}
{}^{n}R^{v} &= \frac{1}{2\omega_n}\langle 0|\mathbf{p}|n\rangle \cdot \langle n|\mathbf{L}|0\rangle \text{ (velocity gauge)} && (3.4)\\
{}^{n}R^{r} &= -\frac{i}{2}\langle 0|\mathbf{r}|n\rangle \cdot \langle n|\mathbf{L}|0\rangle \text{ (length gauge)} && (3.5)
\end{aligned}
$$

In these expressions, atomic units are used. **L**, **p** and **r** refer to the orbital angular momentum, momentum and electronic position operators respectively and $\hbar\omega_n$ refers to the excitation energy for the nth electronic transition [11, 24].

Dipole strength The absorption intensity for a transition from the ground state $|0\rangle$ to the excited state $|n\rangle$ is proportional to the scalar dipole strength and is given by [11]

$$
\begin{aligned}
{}^{n}D^{v} &= \frac{1}{\omega_n^2}\langle 0|\mathbf{p}|n\rangle \cdot \langle n|\mathbf{p}|0\rangle \text{ (velocity gauge)} && (3.6)\\
{}^{n}D^{r} &= \langle 0|\mathbf{r}|n\rangle \cdot \langle n|\mathbf{r}|0\rangle \text{ (length gauge)} && (3.7)
\end{aligned}
$$

3.1.2 Coupled Cluster theory

The ground state CC wave function is given by the ansatz [2, 25]

$$\langle CC\rangle = exp(T)|HF\rangle \tag{3.8}$$

where the reference wave function is a single determinant Hartree-Fock wave function. The cluster operator T is given by

$$T = T_1 + T_2 + \cdots + T_n = \sum_{\mu} \tau_\mu t_\mu \tag{3.9}$$

where T_n,τ_μ, and t_μ refer to n electron excitations, excitation operator and cluster amplitudes respectively and μ denotes the individual excitations.

Multiplying the Schrödinger equation from the left with $exp(-T)$, we obtain

$$exp(-T)Hexp(T)|HF\rangle = E|HF\rangle \tag{3.10}$$

which maybe regarded as a Schrödinger equation with an effective, non-Hermitian similarity-transformed Hamiltonian H^T.

Projecting the similarity-transformed Schrödinger equation onto the Hartree-Fock state and onto the excited projection manifold, we arrive at the equations for the coupled-cluster amplitudes and energy:

$$
\begin{aligned}
\langle HF|exp(-T)Hexp(T)|HF\rangle &= E && (3.11)\\
\langle \mu|exp(-T)Hexp(T)|HF\rangle &= 0 && (3.12)
\end{aligned}
$$

3.1.3 Response theory

Response functions of a system govern the response of the observables of the molecular systems to external frequency-dependent perturbations. The exact response functions have poles where the frequency of an external perturbation is identical to excitation energy[2]. For excited state properties, response theory approach can be used to determine properties related to frequency-dependent electromagnetic fields and non-linear optical spectroscopies [1]. The frequency-dependent response functions can be derived from time-averaged quasienergy. The quasienergy is similar to the energy in time-independent theory. For exact wavefunctions, the time-independent Hellmann-Feynman Theorem is stated as

$$\frac{dE}{d\epsilon} = \frac{d}{d\epsilon}\langle\psi|\hat{H}|\psi\rangle = \langle\psi|\frac{\partial\hat{H}}{\partial\epsilon}|\psi\rangle \tag{3.13}$$

The time-averaged time-dependent Hellmann-Feynman theorem identifies response functions as derivatives of quasienergy.

The variational principle for Time-Periodic Systems is given by

$$\delta\frac{1}{\tau}\int_{t_o}^{t_o+\tau}\langle\tilde{\psi}|\hat{H}(t,\epsilon) - i\frac{d}{dt}|\tilde{\psi}\rangle = 0 \tag{3.14}$$

The derivation of frequency-dependent response properties using Fourier component variational perturbation theory has been reported [1]. Transition strengths are calculated as residues of a linear response function in coupled cluster theory [13, 26].

$$\langle 0|A|n\rangle\langle n|B|0\rangle = \lim_{\omega\to\omega_n}(\omega-\omega_n)\langle\langle A,B\rangle\rangle_\omega \tag{3.15}$$

The rotator strengths can be expressed using response functions [12, 26] as

$$^nR^v = \frac{1}{2\omega_n}\sum_{i=1}^{3}\lim_{\omega\to\omega_n}(\omega-\omega_n)\langle\langle p_i;L_i\rangle\rangle_\omega \text{ (velocity gauge)} \tag{3.16}$$

$$^nR^r = -\frac{i}{2}\sum_{i=1}^{3}\lim_{\omega\to\omega_n}(\omega-\omega_n)\langle\langle r_i;L_i\rangle\rangle_\omega \text{ (length gauge)} \tag{3.17}$$

where $\langle\langle;\rangle\rangle$ denotes the linear response function.

The dipole strengths can be expressed using response functions [11] as

$$
\begin{aligned}
{}^{n}D^{v} &= \frac{1}{\omega_n^2} \lim_{\omega \to \omega_n} (\omega - \omega_n) \langle\langle \mathbf{p}; \mathbf{p} \rangle\rangle_{\omega} \text{ (velocity gauge)} && (3.18)\\
{}^{n}D^{r} &= \lim_{\omega \to \omega_n} (\omega - \omega_n) \langle\langle \mathbf{r}; \mathbf{r} \rangle\rangle_{\omega} \text{ (length gauge)} && (3.19)
\end{aligned}
$$

where $\langle\langle ; \rangle\rangle$ denotes the linear response function.

3.1.4 Coupled Cluster Response Theory [1–3]

The starting point of CC response theory is the Lagrangian[19]

$$L_{CC} = E_{CC} + \sum_{\mu} \bar{t}_{\mu} \Omega_{\mu} \tag{3.20}$$

The excitation energies in CC response theory are determined by

$$
\begin{aligned}
\mathbf{A} R^{i} &= \omega_i R^{i} && (3.21)\\
L^{i} \mathbf{A} &= L^{i} \omega_i && (3.22)
\end{aligned}
$$

where $\mathbf{A}$ is the CC Jacobian which is not symmetric. $\mathbf{A}$ is the partial second derivative of L_{CC} with respect to cluster amplitudes t_{μ} and Lagrange multipliers $\bar{t}_{\mu}$. The right and left eigen vectors, R^{i} and L^{i}, are therefore not adjoints of each other. However, the eigen vectors are biorthogonal and can be chosen to satisfy the normalization condition.

$$L^{i} R^{j} = \delta_{ij} \tag{3.23}$$

The one-photon transition strength for a transition from state m to state n is

$$S_{XY}^{mn} = \langle m|X|n\rangle \langle m|X|n\rangle = \frac{1}{2}[T_{mn}^{X} T_{nm}^{Y} + (T_{nm}^{Y} T_{mn}^{X})^{*}] \tag{3.24}$$

Symmetrization with respect to complex conjugation and simultaneous exchange of X and Y is essential for non-variational models and for exact states it is redundant.

Only the product of two transition matrix elements is unambiguously defined by this equation and CC left and right transition matrix elements cannot be unambiguously ascertained. Thus only ($|\langle m|X|n|^2 = S_{XX}^{mn}$) is determined.

In the CC response theory, the spin-orbit operator is used in the place of operators X and Y. Only the pure singlet and triplet states in the absence of spin-orbit coupling are

considered initially. Then the effects of coupling are introduced and this corresponds to a perturbative treatment. In addition, spin symmetries are exploited to derive equations within a spin-free formalism[19]. For closed-shell reference determinants, the cluster operator T commutes with spin operator S^2 because the states determined by response theory are pure spin states.

3.1.5 Breakdown of Perturbational ansatz[2]

In case of curve-crossings between a reference state and another state, response theory approach fails due to the breakdown of perturbational ansatz. At a crossing, the coupling between two states will no longer be small compared to the energy difference whch leads to the breakdown of perturbational ansatz.

3.1.6 Gauge-origin invariance

In the CCSD theory, gauge invariance is absent and the theory is not origin independent. The excited states in coupled cluster theory being orthogonal to the ground state trivially establish origin independence for the oscillator strength [13].Gauge-origin invariance is observed in velocity gauge formulation of rotatory strength tensor regardless of basis set quality. This is not true in the case of length gauge formulation and leads to errors for approximate calculations[27]. These conclusions can be carried over to scalar rotatory strengths [13].

3.2 Spin free formalism for CPP and Perturbation theory

3.2.1 Treatment of spin-forbidden transitions in PT

The importance of spin-orbit effects increases with increasing nuclear charge but these effects can also become crucial for some aspects of molecular behaviour for systems containing only light atoms[2].The main relativistic corrections for molecules without heavy elements is the first-order spin-orbit correction and the first-order one-electron spin-free corrections [29]. The emission of light in phosphorescence is spin-forbidden in non relativistic quantum mechanics because of the change in spin quantum number

between the excited state and the ground state. For light elements, spin-orbit coupling with perturbation theory presents a sufficiently accurate description of phosphorescence [19].

3.2.2 Spin-free formalism

In all cases, we follow the convention that occupied molecular orbitals are labeled with i,j, ... and virtual molecular orbitals are labeled with a,b, ... MOs that can be either occupied or virtual are labeled with p,q,r, s.

The linear independent basis for one- and two-electron excitation operators is given by

$$^1\tau_{ai} = E_{ai} \tag{3.25}$$

$$^1\tau_{aibj} = E_{ai}E_{bj} \text{ with } (ai) > (bj) \tag{3.26}$$

For closed-shell systems, spin-symmetry can be used to introduce singlet and triplet adapted excitation operators [19, 28].

Case(i): Singlet

$$^3\tau_{ai} = T_{ai} \tag{3.27}$$

$$^{(+)}\tau_{aibj} = T_{ai}E_{bj} + E_{ai}T_{bj} \text{ with } a > b, i > j \tag{3.28}$$

$$^{(-)}\tau_{aibj} = T_{ai}E_{bj} - E_{ai}T_{bj} \text{ with } (ai) > (bj) \tag{3.29}$$

Case(ii): Triplet

$$E_{ai} = a^\dagger_{a\alpha}a_{i\alpha} + a^\dagger_{a\beta}a_{i\beta} \tag{3.30}$$

$$T_{ai} = a^\dagger_{a\alpha}a_{i\alpha} - a^\dagger_{a\beta}a_{i\beta} \tag{3.31}$$

The Hamiltonian and components of dipole operator can be expressed in spin-free form as

$$\tilde{H} = \sum_{pq}\tilde{h}_{pq}E_{pq} + \frac{1}{2}\sum_{pqrs}\tilde{g}_{pqrs}(E_{pq}E_{rs} - \delta_{qr}E_{ps}) \tag{3.32}$$

$$\tilde{X} = \sum_{pq}\tilde{V}^X_{pq}E_{pq} \tag{3.33}$$

3.2.3 Spin-Orbit operator

Spin-orbit coupling constants describe coupling between states of different spin-multiplicity. The spin-orbit coupling constant between singlet state ${}^1m$ and triplet state ${}^3n$ is given by $\langle {}^1m|H_{so}|{}^3n\rangle$ where H_{so} is the spin-orbit operator. The calculations of these matrix elements are non-trivial[2].

The operator which affects both the spin and spatial part of the wave function is called the spin-orbit operator and the effective one-electron spin-orbit coupling operator can be expressed in the second quantization representation [30] as

$$V^{SOC} = \frac{1}{2}\sum_{pq}(V^x_{pq}T^x_{pq} + V^y_{pq}T^y_{pq} + V^z_{pq}T^z_{pq}) \text{ (Cartesian)} \tag{3.34}$$

$$= \frac{1}{2}\sum_{pq}(V^+_{pq}T^{1,-1}_{pq} - V^-_{pq}T^{1,+1}_{pq} + V^z_{pq}T^z_{pq}) \text{ spin-tensor form (Helgaker)} \tag{3.35}$$

$$= \frac{1}{2}\sum_{pq}(-V^{1,+1}_{pq}T^{1,-1}_{pq} - V^{1,-1}_{pq}T^{1,+1}_{pq} + V^{1,0}_{pq}T^{1,0}_{pq}) \text{ spin-tensor form} \tag{3.36}$$

The cartesian components of the triplet excitation operators are given by

$$T^x_{pq} = a^\dagger_{p\alpha}a_{q\beta} + a^\dagger_{p\beta}a_{q\alpha} \tag{3.37}$$

$$T^y_{pq} = \frac{1}{i}(a^\dagger_{p\alpha}a_{q\beta} - a^\dagger_{p\beta}a_{q\alpha}) \tag{3.38}$$

$$T^z_{pq} = a^\dagger_{p\alpha}a_{q\alpha} - a^\dagger_{p\beta}a_{q\beta} \tag{3.39}$$

The prefactor $\frac{1}{2}$ in the Cartesian triplet operators has been moved in front of the summation in the expression for V^{SOC}. Otherwise, these equations directly compare with the equations in reference [30].

In molecular electronic structure theory, a spin tensor operator of integral or half-integral rank S is a set of 2S+1 operators $\hat{T}^{S,M}$ [30]. The three components of the triplet excitation operator in spin tensor form are given by

$$T^{1,-1}_{pq} = a^\dagger_{p\beta}a_{q\alpha} \tag{3.40}$$

$$T^{1,+1}_{pq} = -a^\dagger_{p\alpha}a_{q\beta} \tag{3.41}$$

$$T^{1,0}_{pq} = \frac{1}{\sqrt{2}}(a^\dagger_{p\alpha}a_{q\alpha} - a^\dagger_{p\beta}a_{q\beta}) \tag{3.42}$$

The relations between the Cartesian and spin tensor form of the triplet excitation operators are given by

$$T^x_{pq} = -T^{1,+1}_{pq} + T^{1,-1}_{pq} \tag{3.43}$$

$$T^y_{pq} = \frac{1}{i}(-T^{1,+1}_{pq} - T^{1,-1}_{pq}) \tag{3.44}$$

$$T^z_{pq} = T_{pq} = \sqrt{2}T^{1,0}_{pq} \tag{3.45}$$

The transformation matrix elements between the Cartesian and spin tensor forms can then be obtained from the definition of the triplet excitation operators in these forms. V^{SOC} can be written as

$$V^{SOC} = \frac{1}{2}\sum_{pq}(V^x_{pq} - T^{1,+1}_{pq} + T^{1,-1}_{pq} + V^y_{pq}\frac{1}{i}(-T^{1,+1}_{pq} - T^{1,-1}_{pq}) + V^z_{pq}\sqrt{2}T^{1,0}_{pq}) \tag{3.46}$$

$$= \frac{1}{2}\sum_{pq}((V^x_{pq} + iV^y_{pq})T^{1,-1}_{pq} - (V^x_{pq} - iV^y_{pq})T^{1,+1}_{pq} + \sqrt{2}V^z_{pq}T^{1,0}_{pq}) \tag{3.47}$$

This leads to the following identities

$$V^{1,-1}_{pq} = -(V^x_{pq} + iV^y_{pq}) = -V^+_{pq} \tag{3.48}$$

$$V^{1,+1}_{pq} = -(V^x_{pq} - iV^y_{pq}) = -V^-_{pq} \tag{3.49}$$

$$V^{1,0}_{pq} = \sqrt{2}V^z_{pq} \tag{3.50}$$

3.2.4 Matrix elements of the spin-orbit operator

If the reference states are closed-shell cases , spin symmetry can be utilized to introduce singlet and triplet adapted excitation operators. Both the Hamiltonian and the components of the dipole operator can be expressed in a spin-free form [19]. For spin-forbidden transitions involving a singlet state and triplet state,the triplet state can couple to the singlet state through the three components of the SOC operator.

$$\langle {}^1 0|V^{SOC}|^{3,m_s} f\rangle = \begin{cases} -\frac{1}{2}\sum_{pq} V^{1,+1}_{pq}\langle {}^1 0|T^{1,-1}_{pq}|^{3,+1} f\rangle \\ -\frac{1}{2}\sum_{pq} V^{1,-1}_{pq}\langle {}^1 0|T^{1,+1}_{pq}|^{3,-1} f\rangle \\ \quad +\frac{1}{2}\sum_{pq} V^{1,0}_{pq}\langle {}^1 0|T^{1,0}_{pq}|^{3,0} f\rangle \end{cases} \tag{3.51}$$

The $M_s = 0$ component ($T^z_{pq} = T^{1,0}_{pq}$) does not change the M_s quantum number. A formulation that requires only the $\langle {}^1 0|T_{pq}|^{3,0} f\rangle$ matrix element of the T_{pq} operator can

be found using the Wigner-Eckart theorem. This allows the treatment of singlet-triplet transitions in a spin-free formalism[19].

3.2.5 Wigner-Eckart theorem

The Wigner-Eckart theorem [31] (WET) can be applied to generate equalities where all components of the triplet state are expressed using only the $\langle {}^1 0|T_{pq}|^{3,0} f\rangle$ matrix element of the T_{pq} operator.

With the help of WET

$$\langle j' m'''|T^{kq'}|jm''\rangle = (-1)^{m'''-m'} \frac{\begin{pmatrix} j' & k & j \\ -m''' & q' & m'' \end{pmatrix}}{\begin{pmatrix} j' & k & j \\ -m' & q & m \end{pmatrix}} \langle j' m'|T^{kq}|jm\rangle \tag{3.52}$$

the following equalities can be generated

$$\langle {}^1 0|T^{1,0}_{pq}|^{3,0} f\rangle = \frac{1}{\sqrt{2}}\langle {}^1 0|T_{pq}|^{3,0} f\rangle \tag{3.53}$$

$$\langle {}^1 0|T^{1,-1}_{pq}|^{3,+1} f\rangle = -\langle {}^1 0|T^{1,0}_{pq}|^{3,0} f\rangle = -\frac{1}{\sqrt{2}}\langle {}^1 0|T_{pq}|^{3,0} f\rangle \tag{3.54}$$

$$\langle {}^1 0|T^{1,+1}_{pq}|^{3,-1} f\rangle = -\langle {}^1 0|T^{1,0}_{pq}|^{3,0} f\rangle = -\frac{1}{\sqrt{2}}\langle {}^1 0|T_{pq}|^{3,0} f\rangle \tag{3.55}$$

The matrix elements of the SOC operator can then be expressed as

$$\langle {}^1 0|V^{SOC}|^3 f(M_s = +1)\rangle = \frac{1}{2}\sum_{pq} V^{1,+1}_{pq}\langle {}^1 0|T_{pq}|^{3,0} f\rangle \tag{3.56}$$

$$\langle {}^1 0|V^{SOC}|^3 f(M_s = -1)\rangle = \frac{1}{2}\sum_{pq} V^{1,-1}_{pq}\langle {}^1 0|T_{pq}|^{3,0} f\rangle \tag{3.57}$$

$$\langle {}^1 0|V^{SOC}|^3 f(M_s = 0)\rangle = \frac{1}{2}\sum_{pq} V^{1,0}_{pq}\langle {}^1 0|T_{pq}|^{3,0} f\rangle \tag{3.58}$$

Phosphorescence has been implemented at the MCSCF level using quadratic response functions for singlet and triplet perturbations. The equations obtained here compare well with the equations obtained for MCSCF [20].

3.2.6 Phosphorescence

The spin-forbidden transitions between the excited triplet state $|^3 f\rangle$ and the singlet ground state $|^1 0\rangle$ is called phosphorescence. In order to compute rotator strengths for

circularly polarized phosphorescence, the first-order transition dipole matrix elements between the initial and final states averaged over the M_s components is required. For exact spin eigen functions, the dipole transition moment vanishes for states of different multiplicities. But when spin-orbit interactions are considered, these states are no longer pure spin states [20].

$$\begin{aligned}\sum_m |\langle {}^1 0|\mathbf{r}|^{3,0} f\rangle^{(1)}|^2 &= \sum_m ((\langle {}^1 0|x|^{3,m} f\rangle^{(1)})^* \langle {}^1 0|x|^{3,m} f\rangle^{(1)} \\ &+ (\langle {}^1 0|y|^{3,m} f\rangle^{(1)})^* \langle {}^1 0|y|^{3,m} f\rangle^{(1)} + (\langle {}^1 0|z|^{3,m} f\rangle^{(1)})^* \langle {}^1 0|z|^{3,m} f\rangle^{(1)})\end{aligned} \tag{3.59}$$

Using perturbation theory, the spin contaminants can be expanded in a set of intermediate states to obtain a sum-over state expression for exact states.

$$\begin{aligned}\langle {}^1 0|x|^{3,m} f\rangle^{(1)} &= \sum_{{}^1 k} \frac{\langle {}^1 0|x|{}^1 k\rangle \langle {}^1 k|V^{SOC}|^{3,m} f\rangle}{\omega_f - \omega_k} \\ &- \sum_{{}^{3,m} k} \frac{\langle {}^1 0|V^{SOC}|^{3,m} k\rangle \langle {}^{3,m} k|x|^{3,m} f\rangle}{\omega_k}\end{aligned} \tag{3.60}$$

For the unperturbed states, the excitation energies ω_k for the three components of a triplet ${}^3 k$ do not depend on m. We may rewrite the last equation as

$$\langle {}^1 0|x|^{3,m} f\rangle^{(1)} = \langle {}^1 \tilde{0}_x|V^{SOC}|^{3,m} f\rangle + \langle {}^1 0|V^{SOC}|^{3,m} \tilde{f}_x\rangle \tag{3.61}$$

with the short-hand notation

$$|{}^1 \tilde{0}_x\rangle = \sum_{{}^1 k} |{}^1 k\rangle \frac{\langle {}^1 k|x\langle {}^1 0|}{\omega_f - \omega_k} \tag{3.62}$$

$${}^{3,m} \tilde{f}_x = \sum_{{}^{3,m} k} |{}^{3,m} k\rangle \frac{\langle {}^{3,m} k|x|^{3,m} f\rangle}{-\omega_k} \tag{3.63}$$

We can then express the first-order transition strengths as

$$\sum_m (\langle {}^1 \tilde{0}_x|V^{SOC}|^{3,m} f\rangle + \langle {}^1 0|V^{SOC}|^{3,m} \tilde{f}_x\rangle)^* (\langle {}^1 \tilde{0}_x|V^{SOC}|^{3,m} f\rangle + \langle {}^1 0|V^{SOC}|^{3,m} \tilde{f}_x\rangle) \tag{3.64}$$

Four contributions can be obtained on opening the parentheses, all of the form:

$$\sum_m \langle {}^1i|V^{SOC}|^{3,m}f\rangle^* \langle {}^1j|V^{SOC}|^{3,m}g\rangle \quad (3.65)$$

$$= \frac{1}{4}\sum_{pq,rs}(\langle {}^1i|V_{pq}^{1,+1}T_{pq}^{1,-1}|^{3,+1}f\rangle^* \langle {}^1j|V_{pq}^{1,+1}T_{pq}^{1,-1}|^{3,+1}g\rangle \quad (3.66)$$

$$+\langle {}^1i|V_{pq}^{1,-1}T_{pq}^{1,+1}|^{3,-1}f\rangle^* \langle {}^1j|V_{pq}^{1,-1}T_{pq}^{1,+1}|^{3,-1}g\rangle$$

$$+\langle {}^1i|V_{pq}^{1,0}T_{pq}^{1,0}|^{3,0}f\rangle^* \langle {}^1j|V_{pq}^{1,0}T_{pq}^{1,0}|^{3,0}g\rangle)$$

$$= \frac{1}{4}\sum_{pq,rs}((V_{pq}^{1,+1})^*V_{rs}^{1,+1} + (V_{pq}^{1,-1})^*V_{rs}^{1,-1} + (V_{pq}^{1,0})^*V_{rs}^{1,0}) \quad (3.67)$$

$$\times \langle {}^1i|T_{pq}^{1,0}|^{3,m}f\rangle^* \langle {}^1j|T_{rs}^{1,0}|^{3,m}g\rangle \quad (3.68)$$

$$= \frac{1}{4}\sum_{pq,rs}((V_{pq}^x + iV_{pq}^y)^*(V_{rs}^x + iV_{rs}^y) + (V_{pq}^x - iV_{pq}^y)^*(V_{rs}^x - iV_{rs}^y) + \sqrt{2}(V_{pq}^z)^*\sqrt{2}V_{rs}^z) \quad (3.69)$$

$$\times \langle {}^1i|\frac{1}{\sqrt{2}}T_{pq}|^{3,m}f\rangle^* \langle {}^1j|\frac{1}{\sqrt{2}}T_{rs}|^{3,m}g\rangle \quad (3.70)$$

$$= \frac{1}{4}\sum_{pq,rs}(2(V_{pq}^x)^*V_{rs}^x + 2(V_{pq}^y)^*V_{rs}^y + 2(V_{pq}^z)^*V_{rs}^z)\frac{1}{2}\langle {}^1i|T_{pq}|^{3,m}f\rangle^* \langle {}^1j|T_{rs}|^{3,m}g\rangle \quad (3.71)$$

$$= \frac{1}{4}\sum_{\alpha=x,y,z}\langle {}^1i|\sum_{pq}V_{pq}^\alpha T_{pq}|^{3,m}f\rangle^* \langle {}^1j|\sum_{rs}V_{rs}^\alpha T_{rs}|^{3,m}g\rangle \quad (3.72)$$

The above equations exploited the facts that the formula for the transition strength includes only a summation over the m components of the triplet state and the transition operators do not affect the spin.

The following type of contributions arise when computing the the SOC matrix elements, where we need to account for all components of the triplet state.

$$\begin{aligned}
|\langle {}^1i|V^{SOC}|^3f\rangle|^2 &= \frac{1}{4}\sum_{pq}(\langle {}^1i|V_{pq}^{1,0}T_{pq}|^3f(M_s=0)\rangle)^* \langle {}^1i|V_{pq}^{1,0}T_{pq}|^3f(M_s=0)\rangle & (3.73)\\
&+ (\langle {}^1i|V_{pq}^{1,-1}T_{pq}|^3f(M_s=0)\rangle)^* \langle {}^1i|V_{pq}^{1,-1}T_{pq}|^3f(M_s=0)\rangle\\
&+ (\langle {}^1i|V_{pq}^{1,+1}T_{pq}|^3f(M_s=0)\rangle)^* \langle {}^1i|V_{pq}^{1,+1}T_{pq}|^3f(M_s=0)\rangle\\
&= (\langle {}^1i|V_{pq}^{z}T_{pq}|^3f(M_s=0)\rangle)^* \langle {}^1i|V_{pq}^{z}T_{pq}|^3f(M_s=0)\rangle & (3.74)\\
&+ \frac{1}{2}(\langle {}^1i|V_{pq}^{x}T_{pq}|^3f(M_s=0)\rangle)^* \langle {}^1i|V_{pq}^{x}T_{pq}|^3f(M_s=0)\rangle\\
&+ \frac{1}{2}(\langle {}^1i|V_{pq}^{y}T_{pq}|^3f(M_s=0)\rangle)^* \langle {}^1i|V_{pq}^{y}T_{pq}|^3f(M_s=0)\rangle\\
&+ \frac{1}{2}(\langle {}^1i|V_{pq}^{x}T_{pq}|^3f(M_s=0)\rangle)^* \langle {}^1i|V_{pq}^{x}T_{pq}|^3f(M_s=0)\rangle\\
&+ \frac{1}{2}(\langle {}^1i|V_{pq}^{y}T_{pq}|^3f(M_s=0)\rangle)^* \langle {}^1i|V_{pq}^{y}T_{pq}|^3f(M_s=0)\rangle\\
&= \sum_{\alpha=x,y,z}(\langle {}^1i|V_{pq}^{\alpha}T_{pq}|^3f(M_s=0)\rangle)^* \langle {}^1i|V_{pq}^{\alpha}T_{pq}|^3f(M_s=0)\rangle & (3.75)
\end{aligned}$$

Chapter 4

Computational details

4.1 Basis sets and Methods

Basis sets In the calculations that have been carried out, we have used cc-pVTZ[32], aug-cc-pVDZ,aug-cc-pVTZ,aug-cc-pVQZ, d-aug-cc-pVDZ, d-aug-cc-pVTZ and d-aug-cc-pVQZ basis sets [33].

Methods The start structures of molecules were generated using MOLDEN[35] and TmoleX[36]. The ground state DFT geometry optimizations were performed using B3LYP[37] functional for small molecules and dispersion-corrected[38] B3LYP functional for the larger metal-free chiral aromatic system. A development version of TURBOMOLE[39] package was used for spin-forbidden transition moments and other calculations were performed using TURBOMOLE V7.1[40]. The two component relativitic calculations X2C-HF-SCF and X2C-CC2 were carried out using ridft [41, 42] and ricc2[15, 43] programs respectively without using point group symmetry.

Some of the ground state geometry optimizations, all of the excited state geometry optimizations and transition strengths were determined using RI-CC2. To obtain converged SCF orbitals, dscf [34] module was used before the ricc2 calculation. For the RI approximation, corresponding optimized auxiliary basis sets[44, 45] were used. Frozen-core approximation for all non-valence electrons was used un the correlation and response treatment. Numerical Laplace transformation was used for the one-electron density matrices that involves derivatives of the cluster amplitude or eigen vectors [19].

4.2 Choice of molecules

The chiral molecules were chosen from literature for which DFT values for CD, CPL and CPP were already available [11, 16].

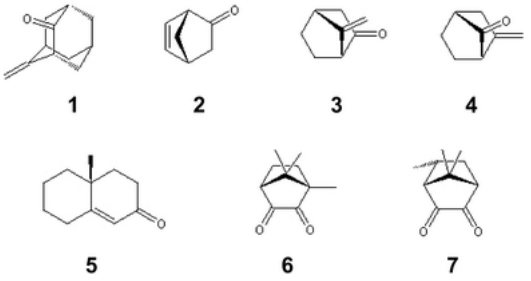


FIGURE 4.1: (1S,3R)-4-methyleneadamantan-2-one **1**, (1R,4R)-bicyclo[2.2.1]hept-5-en-2-one **2**, (1R)-7-methylenebicyclo[2.2.1]heptan-2-one **3**, (1S)-2-methylenebicyclo[2.2.1]heptan-7-one **4**, (R)-(-)4,4a,5,6,7,8-hexahydro-4a-methyl-2(3H)-naphthalenone **5**, (1S,4R)-1,7,7-trimethylbicyclo[2.2.1]heptane-2,3-dione (camphorquinone, **6**), (1S,4R,5R)-5,7,7 trimethylbicyclo[2.2.1]heptane-2,3-dione **7** [16]

Furthermore, to show the applicability of our method to larger systems, a metal-free chiral aromatic system exhibiting CPP, CPF and CD at room temperature reported was chosen from literature[22].

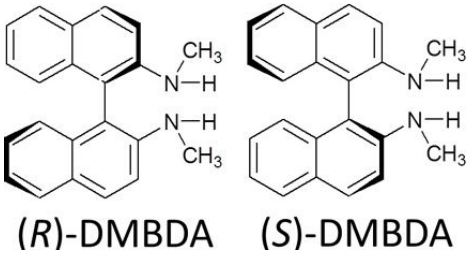


FIGURE 4.2: Structures of (R)-DMBDA((R)-N, N'-dimethyl-1, 1′-binaphthyldiamine) and (S)-DMBDA((S)-N, N'-dimethyl-1, 1′-binaphthyldiamine)[22]

Chapter 5

Results and Discussion

5.1 Test calculations

A small test molecule, Hydrogen Peroxide, was selected [16] to run test calculations to determine the basis set quality and size dependency of calculated dipole strengths and rotational strengths for spin-forbidden transitions using RI-CC2 method. The triplet excited states (π^*, σ^*) of H_2O_2 are valence states with small rydberg character [46]. Diffuse functions are required to study rydberg states which necessitates the use of augmented basis.

TABLE 5.1: Comparison of the RI-CC2 velocity (D^v, R^v) and length (D^l, R^l) gauge results for the dipole $[esu^2\ cm^2]$ and rotational $[esu\ cm\ erg\ G^{-1}]$ strengths of the first spin-forbidden transition in H_2O_2 for the DFT optimized structure using different basis sets.

Basis set	D^l	D^v	R^l	R^v
aug-cc-pVDZ	8.73×10^{-41}	5.03×10^{-41}	-7.49×10^{-46}	-1.45×10^{-44}
aug-cc-pVTZ	9.83×10^{-41}	6.58×10^{-41}	-7.65×10^{-46}	-1.46×10^{-44}
aug-cc-pVQZ	1.02×10^{-40}	7.37×10^{-41}	-8.12×10^{-46}	-1.43×10^{-44}

In the ground state, H_2O_2 belongs to C_2 point group and point group symmetry was exploited in the calculations. Since, the calculations were done on the ground state structures, these calculations correspond to spin-forbidden CD. Dipole strengths and rotational strengths were computed on ground state DFT (B3LYP) geometry optimized structure using different basis sets (Table 5.1). It is observed that the rotational are not

very sensitive to basis set size. The dipole strengths increase slightly with increasing basis set quality. The values for aug-cc-pVQZ are not so different from that of aug-cc-pVDZ.

TABLE 5.2: Comparison between X2C-CC2 and RI-CC2 transition strengths in atomic units

Method	Oscillator Strength	Rotational Strength
X2C-CC2	1.68×10^{-6}	-4.40×10^{-7}
RI-CC2	3.60×10^{-6}	-5.47×10^{-7}

Since no experimental data is available for spin-forbidden CD rotator strengths in H_2O_2, the SOC-PT-CC2 calculation was compared with the relativistic 2-component calculation, which includes the SOC already at the SCF level. In the X2C calculation, only the one-electron part of the spin-orbit Hamiltonian is included. For a better comparison with the 2-component calculations one should disable the 2-electron contribution of the spin-orbit mean-field operator in the non-relativistic calculation. For the cc-pVTZ basis set, the agreement of the relativistic calculation with the perturbative calculation is for the rotational strength as good as for the oscillator strength.

TABLE 5.3: Comparison of the RI-CC2 velocity (D^v, R^v) and length (D^l, R^l) gauge results for the dipole $[esu^2\ cm^2]$ and rotational $[esu\ cm\ erg\ G^{-1}]$ strengths of the first spin-forbidden transition in H_2O_2 for the CC2 optimized ground state structure using different basis sets.

Basis set	D^l	D^v	R^l	R^v
aug-cc-pVDZ	8.37×10^{-41}	5.10×10^{-41}	6.32×10^{-46}	-9.80×10^{-45}
aug-cc-pVTZ	9.38×10^{-41}	6.74×10^{-41}	8.31×10^{-46}	-8.86×10^{-45}
aug-cc-pVQZ	9.70×10^{-41}	7.54×10^{-41}	8.25×10^{-46}	-8.31×10^{-45}
d-aug-cc-pVDZ	8.39×10^{-41}	5.02×10^{-41}	6.36×10^{-46}	-8.91×10^{-45}
d-aug-cc-pVTZ	9.39×10^{-41}	6.75×10^{-41}	8.28×10^{-46}	-8.83×10^{-45}
d-aug-cc-pVQZ	9.69×10^{-41}	7.56×10^{-41}	8.26×10^{-46}	-8.31×10^{-45}

For the CC2 geometry optimized ground state, the values varied as seen in table 5.3. The effect is more for the length gauge results than the velocity gauge results. Dipole strengths remain similar but length gauge rotator strengths also change the sign. Double augmentation does not vary the results significantly. The aug-cc-pVDZ basis set provides sufficient accuracy for the rotational strengths and shall be used to determine rotational strengths for the molecules under study in this master project.

Furthermore, calculations were done both in the velocity gauge and length gauge formulations for the singlet-triplet transitions of first three excited states to establish gauge-origin invariance for the velocity gauge formulation. The length gauge results are origin dependent as expected. Here, two sets of calculations were performed. In one case, the gauge origin was placed at the center of mass which is the default and in the other case the origin was moved away with respect to centre of mass by (1,1,1) vector. The relative changes in the length gauge and velocity gauge results for the DFT optmized ground state (Table 5.4) and CC2 optimized ground state (Table 5.5) are similar. The CC2 geometry optimizations were performed in the respective basis in which the spin-forbidden strengths were determined.

When calculations were redone after the atoms were moved back to the origin, the results were very slightly different from the values calculated initially (values varied in the fourth decimal place). This is attributed to HF orbital artifact.

Since the rotational strength values are reported only upto two decimal places, the velocity-gauge formulation provides sufficient accuracy for gauge-invariance and is used in all further calculations of rotational strengths.

TABLE 5.4: Gauge-origin dependence of rotational [$esu\ cm\ erg\ G^{-1}$] strengths in length gauge and velocity gauge formulations for the first, second and third transitions in H_2O_2 for the DFT geometry optimized ground state structure. CM refers to gauge origin placed in the center of mass , and CM + 1 where it is moved by the (1, 1, 1) vector.

Basis set	Length		Velocity	
	CM	CM + 1	CM	CM + 1
aug-cc-pVDZ	$-7.492\,87 \times 10^{-46}$	$1.401\,09 \times 10^{-46}$	$-1.454\,24 \times 10^{-44}$	$-1.454\,28 \times 10^{-44}$
aug-cc-pVTZ	$-7.647\,74 \times 10^{-46}$	$-9.817\,12 \times 10^{-47}$	$-1.455\,42 \times 10^{-44}$	$-1.455\,47 \times 10^{-44}$
aug-cc-pVQZ	$-8.127\,26 \times 10^{-46}$	$-1.850\,73 \times 10^{-46}$	$-1.435\,28 \times 10^{-44}$	$-1.435\,52 \times 10^{-44}$
aug-cc-pVDZ	$-2.620\,12 \times 10^{-43}$	$-2.619\,43 \times 10^{-43}$	$-1.185\,12 \times 10^{-41}$	$-1.185\,02 \times 10^{-41}$
aug-cc-pVTZ	$-1.320\,67 \times 10^{-43}$	$-1.322\,91 \times 10^{-43}$	$-8.312\,69 \times 10^{-42}$	$-8.312\,09 \times 10^{-42}$
aug-cc-pVQZ	$-8.313\,22 \times 10^{-44}$	$-8.340\,29 \times 10^{-44}$	$-6.799\,02 \times 10^{-42}$	$-6.796\,80 \times 10^{-42}$
aug-cc-pVDZ	$-1.786\,89 \times 10^{-47}$	$9.169\,00 \times 10^{-48}$	$-8.851\,18 \times 10^{-46}$	$-8.856\,30 \times 10^{-46}$
aug-cc-pVTZ	$-6.509\,13 \times 10^{-46}$	$-5.832\,22 \times 10^{-46}$	$5.387\,59 \times 10^{-45}$	$5.386\,96 \times 10^{-45}$
aug-cc-pVQZ	$-8.567\,19 \times 10^{-46}$	$-7.235\,44 \times 10^{-46}$	$1.357\,22 \times 10^{-44}$	$1.357\,13 \times 10^{-44}$

TABLE 5.5: Gauge-origin dependence of rotational [$esu\ cm\ erg\ G^{-1}$] strengths in length gauge and velocity gauge formulations for the first, second and third transitions in H_2O_2 for the CC2 geometry optimized ground state structure. CM refers to gauge origin placed in the center of mass , and CM + 1 where it is moved by the (1, 1, 1) vector.

Length			Velocity	
Basis set	CM	CM + 1	CM	CM + 1
aug-cc-pVDZ	$6.318\,93 \times 10^{-46}$	$1.010\,99 \times 10^{-45}$	$-9.802\,40 \times 10^{-45}$	$-9.802\,27 \times 10^{-45}$
aug-cc-pVTZ	$8.306\,81 \times 10^{-46}$	$1.024\,06 \times 10^{-45}$	$-8.855\,61 \times 10^{-45}$	$-8.855\,95 \times 10^{-45}$
aug-cc-pVQZ	$8.253\,16 \times 10^{-46}$	$1.006\,19 \times 10^{-45}$	$-8.312\,97 \times 10^{-45}$	$-8.313\,69 \times 10^{-45}$
aug-cc-pVDZ	$-3.269\,02 \times 10^{-43}$	$-3.271\,65 \times 10^{-43}$	$-1.755\,21 \times 10^{-41}$	$-1.755\,31 \times 10^{-41}$
aug-cc-pVTZ	$-1.253\,09 \times 10^{-43}$	$-1.258\,16 \times 10^{-43}$	$-8.695\,61 \times 10^{-42}$	$-8.694\,78 \times 10^{-42}$
aug-cc-pVQZ	$-5.306\,64 \times 10^{-44}$	$-5.361\,14 \times 10^{-44}$	$-4.567\,90 \times 10^{-42}$	$-4.567\,37 \times 10^{-42}$
aug-cc-pVDZ	$-8.391\,67 \times 10^{-46}$	$-8.495\,49 \times 10^{-46}$	$-7.995\,42 \times 10^{-45}$	$-7.994\,87 \times 10^{-45}$
aug-cc-pVTZ	$-2.042\,00 \times 10^{-45}$	$-2.038\,56 \times 10^{-45}$	$-2.164\,22 \times 10^{-44}$	$-2.164\,40 \times 10^{-44}$
aug-cc-pVQZ	$-2.447\,60 \times 10^{-45}$	$-2.437\,23 \times 10^{-45}$	$-2.735\,00 \times 10^{-44}$	$-2.735\,28 \times 10^{-44}$

5.2 CPL

The equilibrium geometries of ground state and excited state are important for determining strengths of CD and CPL respectively. When the two structures are similar, the emission and absorption band have same sign and similar magnitude, due to the fact that the rotatory strengths are similar [11].

But, when the excited state has a lifetime long enough for the molecule to structurally relax, CD and CPL bands are dissimilar. CPL spectra with different signs have been reported [11] using DFT methods for β,γ-enones for spin-allowed transitions. This is attributed to the puckering of carbonyl group in the excited state either towards or away from C=C double bond causing an inversion in sign of CPL with respect to CD.

More recently, similar results have been reported for CPP using TDDFT [16] as a probe of the structure of triplet excited states. In the following sections. RI-CC2 calculations have been compared with the DFT results reported in literature [11, 16].

The CD spectrum values did not vary much based on geometry optimization. For example, the spin-forbidden rotational strengths of enone **5** in absorption was $6.794\,91 \times 10^{-44}$ $esu\ cm\ erg\ G^{-1}$ and $6.790\,84 \times 10^{-44}$ $esu\ cm\ erg\ G^{-1}$ for the CC2 and DFT geometry optimized structures respectively.

In all further calculations, the ground state geometry optimization was done using DFT/B3LYP(cc-pVTZ basis set), excited state geometry optimization was done using CC2(aug-cc-pVDZ basis set) and transition strengths were calculated using CC2(aug-cc-pVDZ basis set) unless mentioned otherwise.

5.3 CPF and CPP of β, γ-enones

TABLE 5.6: Comparison of the rotational [*esu cm erg* G^{-1}]strengths in velocity gauge for singlet-singlet transitions in enones using RI-CC2 method and aug-cc-pVDZ basis set.

Strength	Gr	S1a	S1b
Enone 1	1.20×10^{-39}	3.15×10^{-40}	-1.23×10^{-40}
Enone 2	4.25×10^{-39}	1.26×10^{-39}	3.96×10^{-40}
Enone 3	2.34×10^{-39}	5.08×10^{-40}	6.56×10^{-40}
Enone 4	-2.03×10^{-39}	-5.80×10^{-40}	1.95×10^{-41}

The CPF results compare well with the results from DFT [11]. The carbonyl group is flat in the ground state structure. For enone 2, a second excited state minimum was also found using RI-CC2. Enone 3 did not exhibit opposite signs as expected from DFT results. This is possibly due to exchange of closely lying excited states between DFT and CC2.

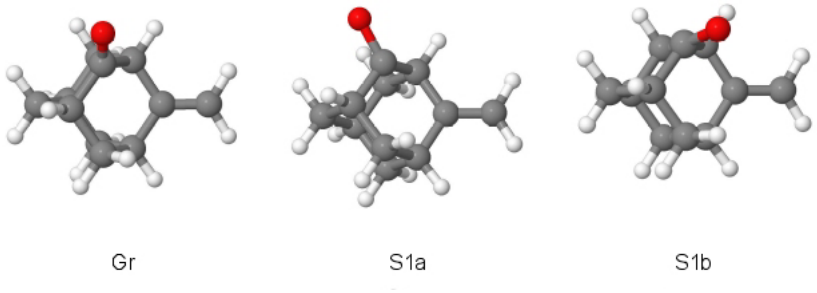


FIGURE 5.1: The ground and first singlet excited state structures of (1S,3R)-4-methyleneadamantan-2-one **1**

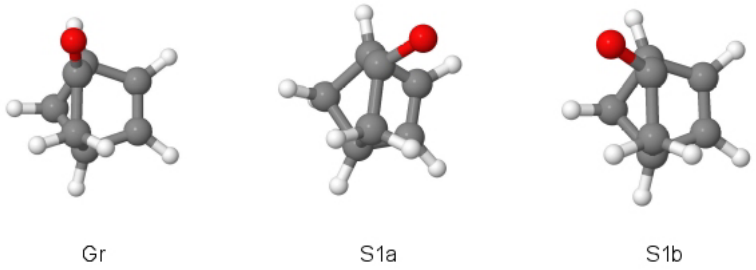


FIGURE 5.2: The ground and first excited singlet state structures of(1R,4R)-bicyclo[2.2.1]hept-5-en-2-one **2**

The most dominant natural transition orbital for the transitions from excited state to ground state is also shown. Natural transition orbitals provide a compact orbital

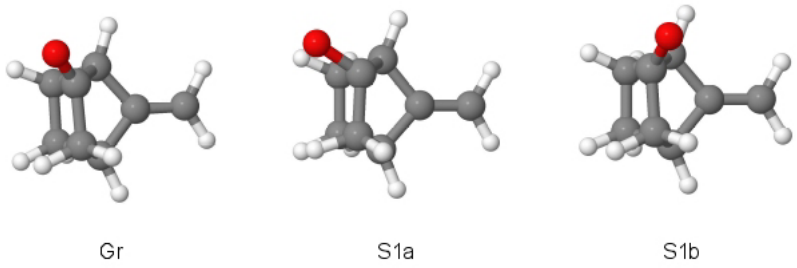


FIGURE 5.3: The ground and first excited singlet state structures of (1R)-7-methylenebicyclo[2.2.1]heptan-2-one **3**

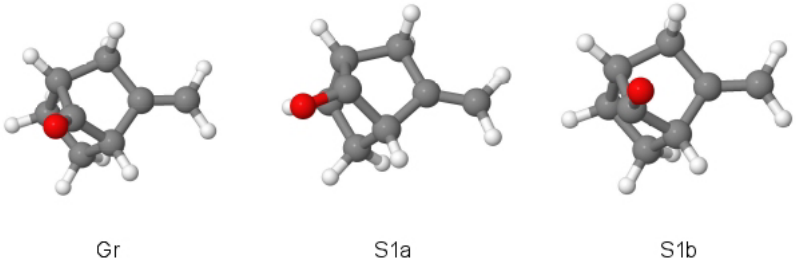


FIGURE 5.4: The ground and first excited singlet state structures of (1S)-2-methylenebicyclo[2.2.1]heptan-7-one **4**

representation for the electron transition density matrix[47]. Here, we can visualize the $n \rightarrow \pi^*$ and $\pi^* \rightarrow n$ nature of the transitions. The RI-CC2 optimization of excited states overestimates carbonyl bond length when compared to DFT [11] and may give rise to discrepancy of the results.The equilibrium geometries of ground state and excited state are important for determining strengths of CD and CPL respectively. The DFT results for CPF show that rotatory strength is sensitive to geometric parameters such as dihedral angles and bond lengths of the chromophores.

For cases, where change in CPL sign is not observed, the NTO's appear similar for both the structures. Since, NTO's are dependent on transition moments which are used to calculate rotator strengths they give rise to qualitatively similar results. The orbitals involved in the $n \rightarrow \pi^*$ excitation are to some extent delocalized on the C=C bond as hypothesized in reference [11].

Similar calculations and NTO analysis have been done for CPP. Our results compare well with DFT [16]. Enone 1 and Enone 4 do not show opposite signs for CPP in the excited states. Enone 2 showed opposite signs to what is expected. This is possibly due to exchange of order of close-lying excited states between DFT and CC2. The triplet excited states look similar to singlet excited states with the puckering of carbonyl either

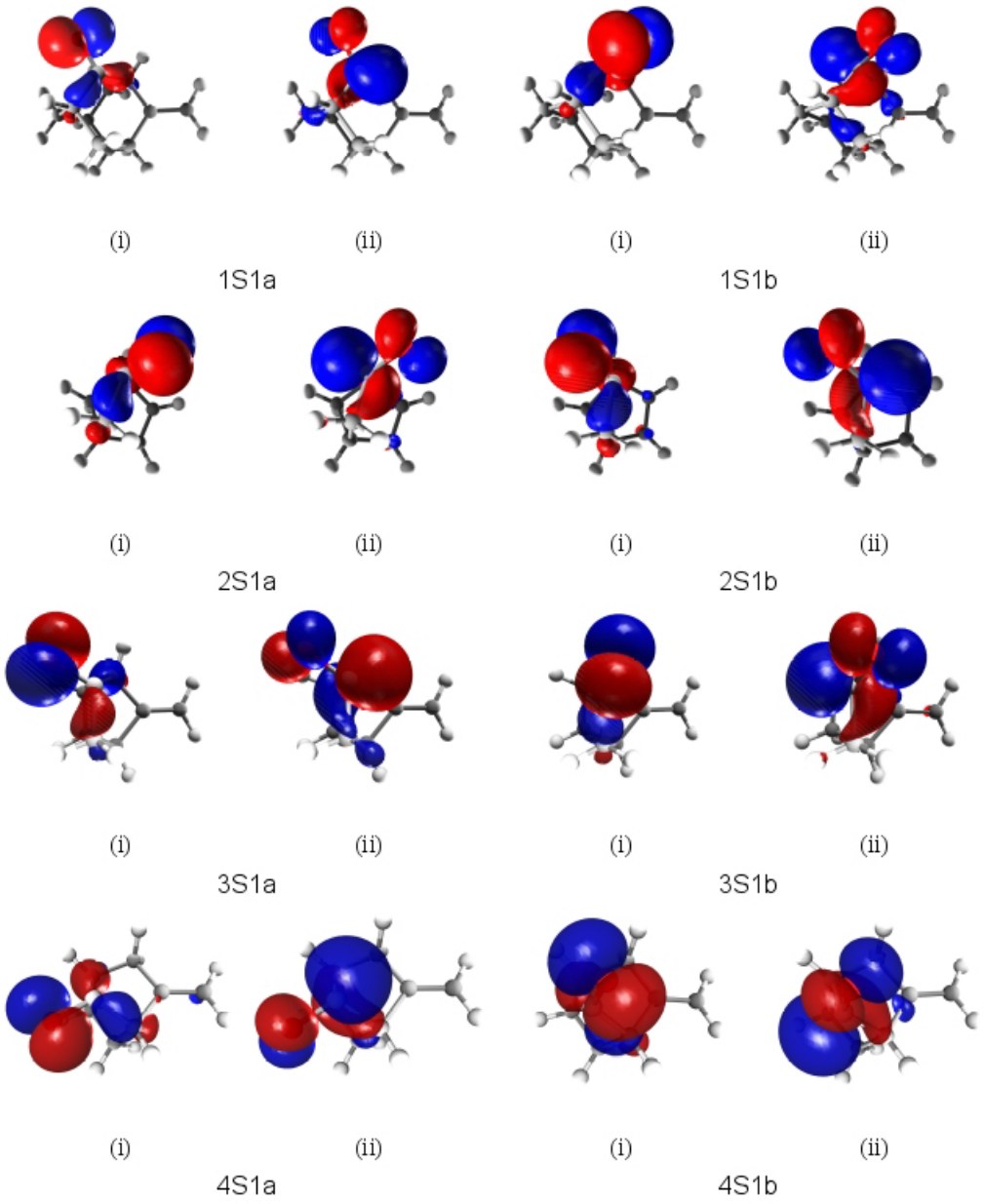


FIGURE 5.5: Most dominant occupied (i) and virtual (ii) natural transition orbitals of enones **1-4** for the singlet excited state structures

towards or away from the C=C bond. The NTO analysis also revealed that T1a state for Enone 2 involved the excitation of C=C chromophore. The NTOs indicate local excitation of the carbonyl chromophore in all cases except for T1a of enone **2** which involves a charge-transfer excitation. When the structures of ground and excited state are similar, the signs of rotator strengths are also similar.

Two local minima were found in the excited state structures both for CPP and CPF. The

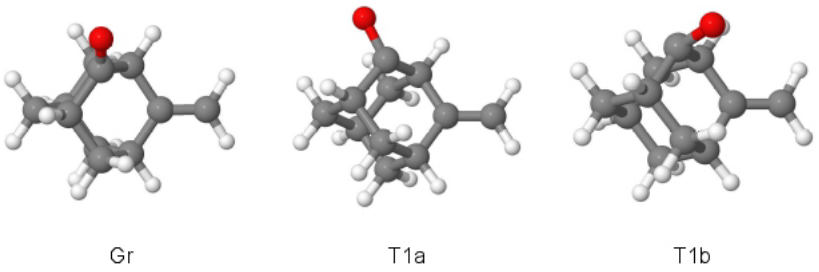


FIGURE 5.6: The ground and first triplet excited state structures of (1S,3R)-4-methyleneadamantan-2-one **1**

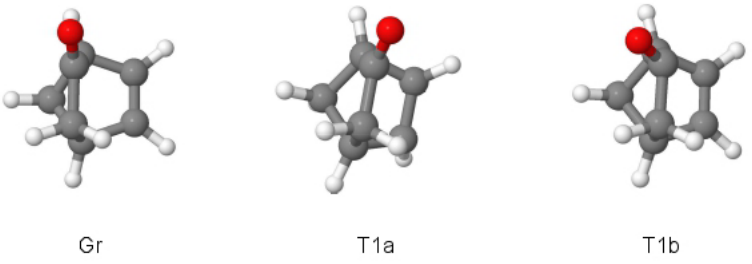


FIGURE 5.7: The ground and first excited triplet state structures of(1R,4R)-bicyclo[2.2.1]hept-5-en-2-one **2**

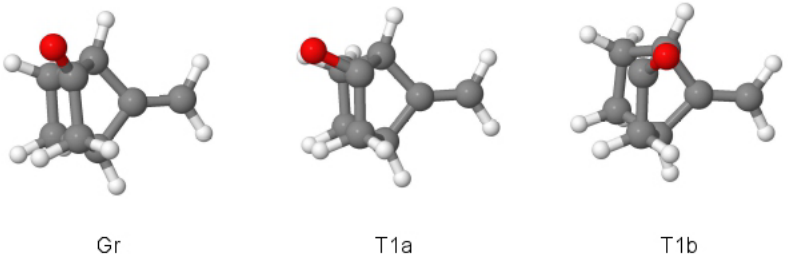


FIGURE 5.8: The ground and first excited triplet state structures of (1R)-7-methylenebicyclo[2.2.1]heptan-2-one **3**

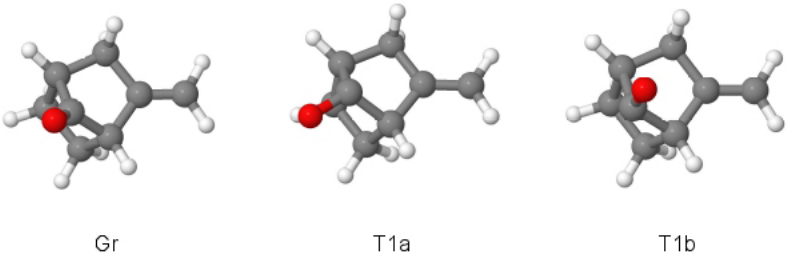


FIGURE 5.9: Most dominant occupied (i) and virtual (ii) natural transition orbitals of enones **1**-**4** for the triplet excited state structures

energies of the two minima do not differ by more than 0.05 eV except for the case where different chromophores are excited (Table 5.7). In all cases, CPP rotational strengths are atleast four orders of magnitude smaller than the corresponding CPF rotational strengths.

TABLE 5.7: Vertical transition energies for CD,CPF and CPP for transitions between ground and first excited state ΔE (eV)

Strength	Gr → T1	T1a	T1b	Gr → S1	S1a	S1b
Enone 1	3.95	2.05	2.05	4.35	2.41	2.45
Enone 2	3.85	1.04	1.93	4.30	2.54	2.44
Enone 3	3.81	2.08	2.06	4.17	2.50	2.55
Enone 4	3.96	1.80	1.79	4.37	2.35	2.36

TABLE 5.8: Comparison of the dipole [esu^2 cm^2] and rotational [esu cm erg G^{-1}]strengths in velocity gauge for singlet-triplet transitions in enones using RI-CC2 method and aug-cc-pVDZ basis set.

Strength	Gr	T1a	T1b
Enone 1			
D	1.57×10^{-41}	1.71×10^{-41}	1.81×10^{-41}
R	-3.43×10^{-45}	-6.27×10^{-45}	-6.56×10^{-45}
Enone 2			
D	8.69×10^{-42}	1.08×10^{-42}	2.18×10^{-41}
R	-1.00×10^{-44}	1.70×10^{-45}	-9.71×10^{-46}
Enone 3			
D	1.60×10^{-41}	8.26×10^{-42}	1.33×10^{-41}
R	6.87×10^{-45}	2.05×10^{-44}	-8.64×10^{-45}
Enone 4			
D	9.15×10^{-42}	2.66×10^{-41}	2.71×10^{-41}
R	8.43×10^{-47}	3.64×10^{-45}	1.74×10^{-45}

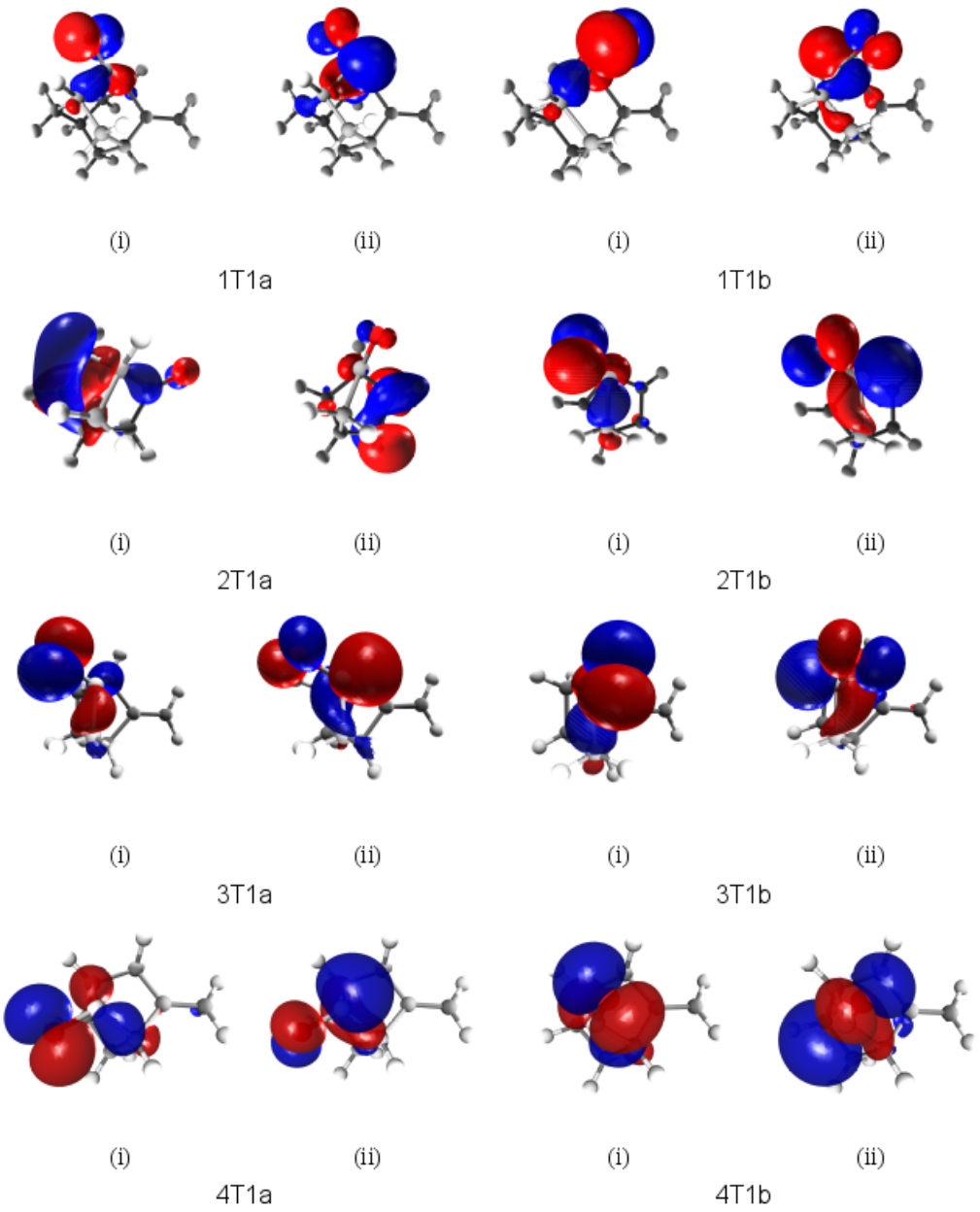


FIGURE 5.10: Most dominant occupied (i) and virtual (ii) natural transition orbitals of enones **1**-**4** for the triplet excited state structures

5.4 Ketones with conjugated double bonds

Molecule **5** is an α, β - enone with conjugated double bonds. The molecule here is an enantiomer and CD results compare well with DFT. The CPP result of the first excited state is opposite to that of DFT result and could be because of exchange of states between DFT and CC2. The 2nd excited state in CD is 0.5 eV higher making this very likely. Here, there is no puckering of carbonyl group in the excited state and it is still flat. The sign of the rotational strength is therefore dependent on the bond lengths and not just the dihedral angle.

TABLE 5.9: The dipole [$esu^2\ cm^2$] and rotational [$esu\ cm\ erg\ G^{-1}$]strengths in velocity gauge for singlet-triplet transitions in enone **5** using RI-CC2 method and aug-cc-pVDZ basis set.

Enone 5	D	R
Absorption	8.02×10^{-41}	6.79×10^{-44}
Emission	1.59×10^{-40}	2.47×10^{-43}

Molecules **6** and **7** are diketones with conjugated double bonds. For the first three excited states, the CD and CPL results have been tabulated for both spin-allowed and spin-forbidden transitions Table 5.10. One would expect that the sign of the rotational strength is same in CD and CPL. But this is not true for all cases. However, this can be explained when one looks at the close lying energy values (Table 5.11) in CPL ($\leq$0.5 eV). There might be an exchange of states in the emission resulting in varying signs.

TABLE 5.10: The rotational [$1 \times 10^{-40}\ esu\ cm\ erg\ G^{-1}$]strengths in velocity gauge for CD,CPF and CPP transitions in diketones **6** and **7** using RI-CC2 method and aug-cc-pVDZ basis set.

Excited state	Absorption (CD)	Emission (CPL)	Excited state	Absorption (spin-forbidden CD)	Emission (CPP)
Diketone 6					
S1	-1.01	1.13	T1	2.75×10^{-6}	-7.52×10^{-6}
S2	0.30	-0.17	T2	2.53×10^{-5}	1.34×10^{-5}
S3	13.84	26.56	T3	-4.45×10^{-5}	-1.08×10^{-4}
Diketone 7					
S1	-0.95	-0.80	T1	5.45×10^{-6}	-1.08×10^{-5}
S2	0.70	0.39	T2	1.76×10^{-5}	-8.55×10^{-5}
S3	3.09	-2.13	T3	-3.69×10^{-5}	9.55×10^{-5}

Also, since no puckering of carbonyl group happens in the excited states, it is clear that puckering cannot be the only reason for sign change in CD and CPL as hypothesized in reference [16]. The NTOs of the first two excited states look very similar for diketones.

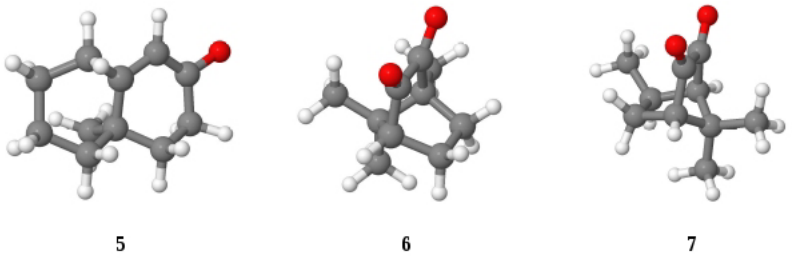


FIGURE 5.11: The first excited triplet state structures of (S)-(-)4,4a,5,6,7,8-hexahydro-4a-methyl-2(3H)-naphthalenone **5**, (1S,4R)-1,7,7-trimethylbicyclo[2.2.1]heptane-2,3-dione (camphorquinone, **6**) and (1S,4R,5R)-5,7,7 trimethylbicyclo[2.2.1]heptane-2,3-dione **7**

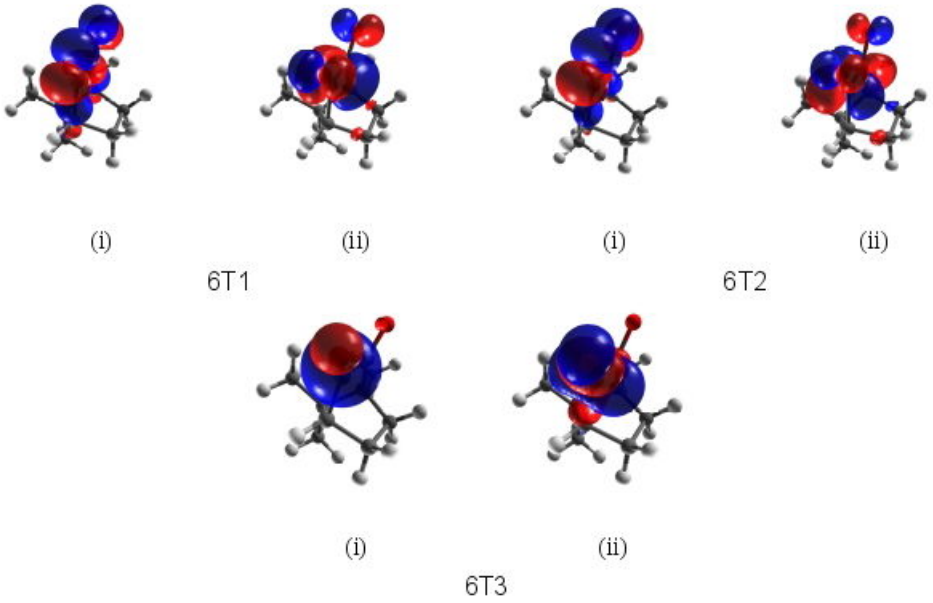


FIGURE 5.12: Most dominant occupied (i) and virtual (ii) natural transition orbitals for the triplet excited state structures of (1S,4R)-1,7,7-trimethylbicyclo[2.2.1]heptane-2,3-dione (camphorquinone, **6**)

It is also seen that the absolute value of rotational strength for the third excited state is always higher than the first two excited states. In some cases it is one or two orders of magnitude higher. This is possibly due to $\pi \rightarrow \pi^*$ transitions which have higher strengths than $n \rightarrow \pi^*$ transitions. In order to emphasize the effect of order of magnitude of rotational strengths on the appearance of the CD spectrum, a CD spectrum for the spin-allowed transitions of Diketone **6** has been included (Figure 5.13).

TABLE 5.11: Vertical transition energies for CD,CPF and CPP for transitions between ground and first, second, third excited states ΔE (eV) in velocity gauge in diketones **6** and **7** using RI-CC2 method and aug-cc-pVDZ basis set.

Excited state	Absorption (CD)	Emission (CPL)	Excited state	Absorption (spin-forbidden CD)	Emission (CPP)
Diketone 6					
S1	3.82	2.29	T1	3.82	2.29
S2	4.93	2.62	T2	4.93	2.62
S3	5.91	4.49	T3	5.91	4.49
Diketone 7					
S1	3.79	2.29	T1	3.79	2.29
S2	5.00	2.57	T2	5.00	2.57
S3	5.48	4.26	T3	5.48	4.26

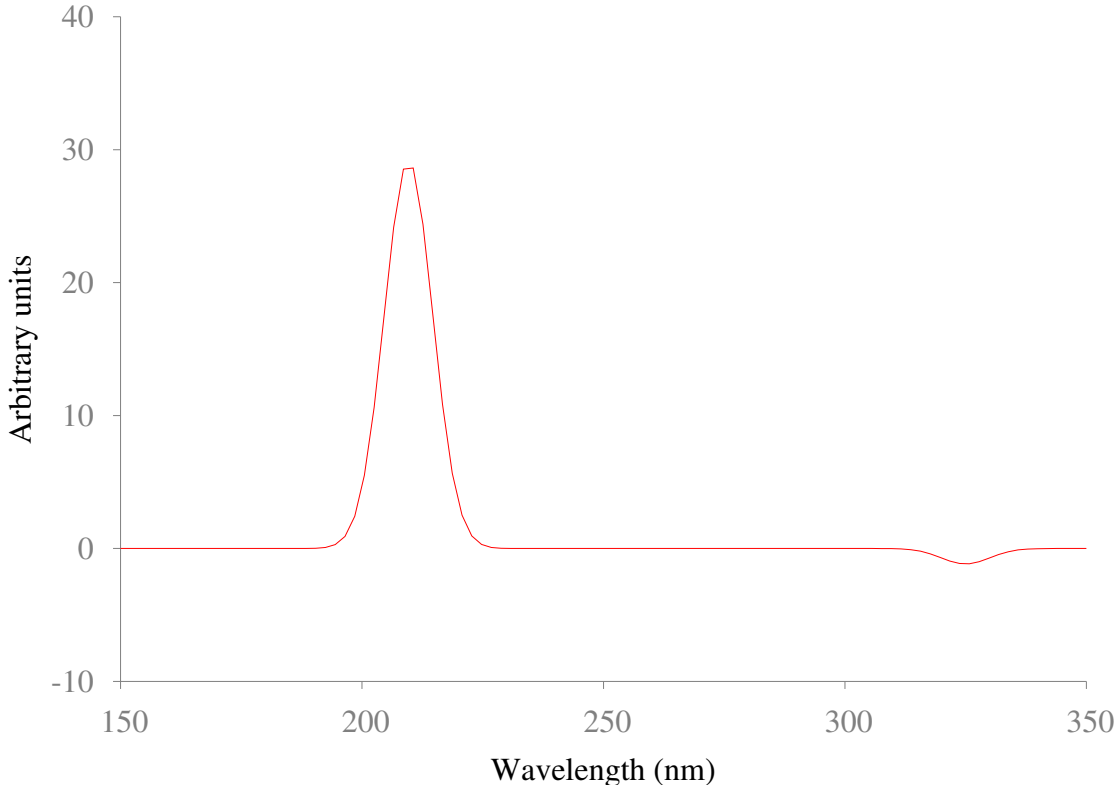


FIGURE 5.13: The CD spectrum for singlet transitions of (1S,4R)-1,7,7-trimethylbicyclo[2.2.1]heptane-2,3-dione (camphorquinone, **6**)

5.5 CPP in Metal-Free Chiral Aromatics

The applicability of SOC-PT-CC2 can be extended to a larger metal-free chiral aromatic system (44 atoms). The molecule, (S)-DMBDA ((S)-N, N'-dimethyl-1, 1′-binaphthyldiamine), exhibits circularly-polarized persistent room-temperature phosphorescence[22].

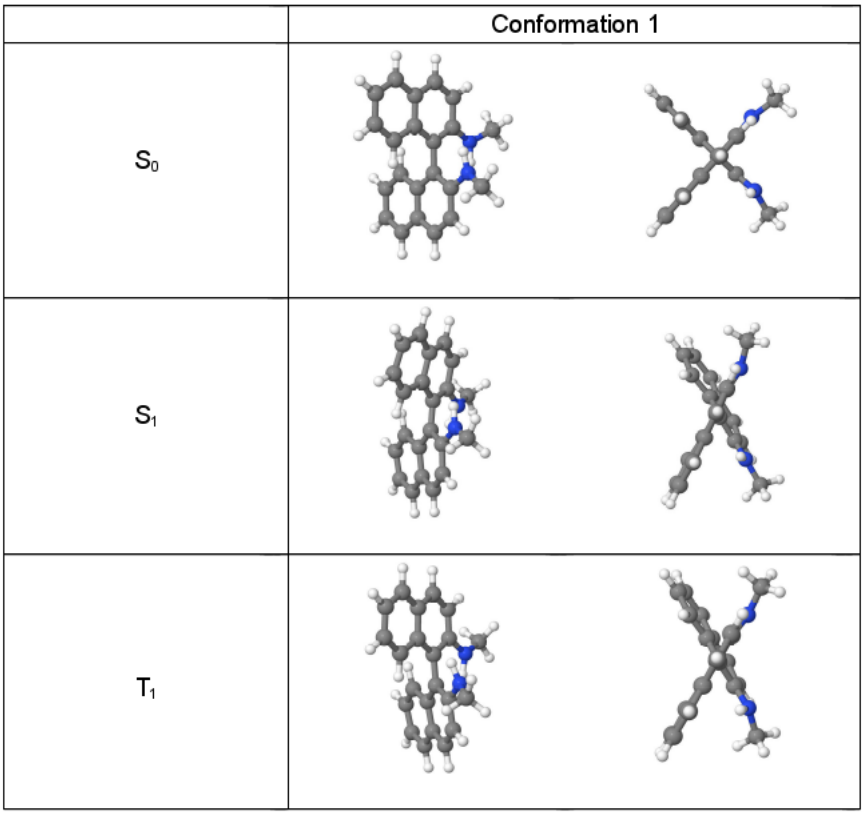


FIGURE 5.14: The geometry-optimized ground state (S_0), first excited singlet state (S_1) and first excited triplet state (T_1) structures of (S)-DMBDA

The enantiomer of this molecule has three conformations each in the ground and first excited singlet state according to the DFT calculations in reference [22]. Calculations for CPL and CD were done using RI-CC2 for one of the conformers of (S)-DMBDA. The geometry optimizations of the ground state structure was performed using DFT/B3LYP(cc-pVTZ) and the excited state structures were geometry optimized using RI-CC2(aug-cc-pVDZ). All the rotational strengths were calculated using RI-CC2 in aug-cc-pVDZ basis set. The rotational strengths calculated from RI-CC2 (Table 5.12)

agreed qualitatively with the TD-DFT results for the enantiomer. RI-CC2 underestimated the rotational strengths by a factor of one when compared to TD-DFT. Figure 5.14 also shows the geometry optimized triplet excited state using RI-CC2 (aug-cc-pVDZ). The excited state geometries agree well with that of DFT optimized structures.

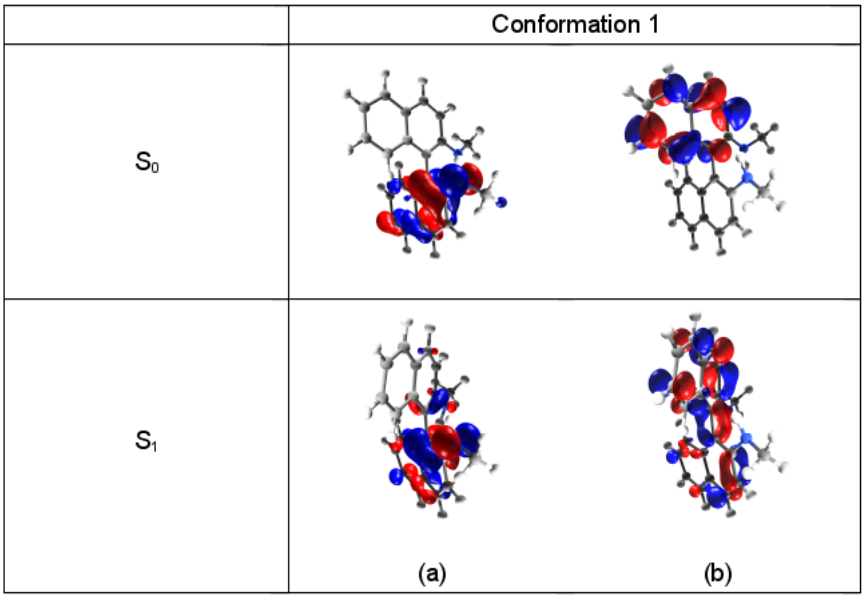


FIGURE 5.15: Most dominant occupied (a) and virtual (b) natural transition orbitals of (S)-DMBDA for the transition from ground state to first excited state as visualized on the ground state (S_0) structure and first excited state(S_1) structure

The NTOs for the singlet-singlet transitions show charge-transfer from one binaphthyl to the other. Since, S-DMBDA is C2-symmetric another set of NTOs with an opposite charge-transfer between binaphthyls was expected. A second close-lying excited state($\Delta E \approx 0.1$ eV) to this effect was found using RI-CC2 with an opposite sign for the rotational strength of spin-allowed CD.

The rotational strength calculated for the spin-forbidden triplet-singlet tansition using SOC-PT-CC2 was 5.96×10^{-47} $esu\ cm\ erg\ G^{-1}$. Experimentally, the phosphorescence is observed between 500-600 nm which agrees well with our result at $\approx$ 556 nm corresponding to the yellow region of the visible spectrum. The NTOs (Figure 5.17) for CPP exhibit local excitations in contrast to charge-transfer excitations observed in CPF.

Thus, SOC-PT-CC2 approach can be used to calculate spin-forbidden rotational strengths of larger molecules. With its low computational costs, RI-CC2 is useful for computing the CPP rotational strengths of large metal-free systems.

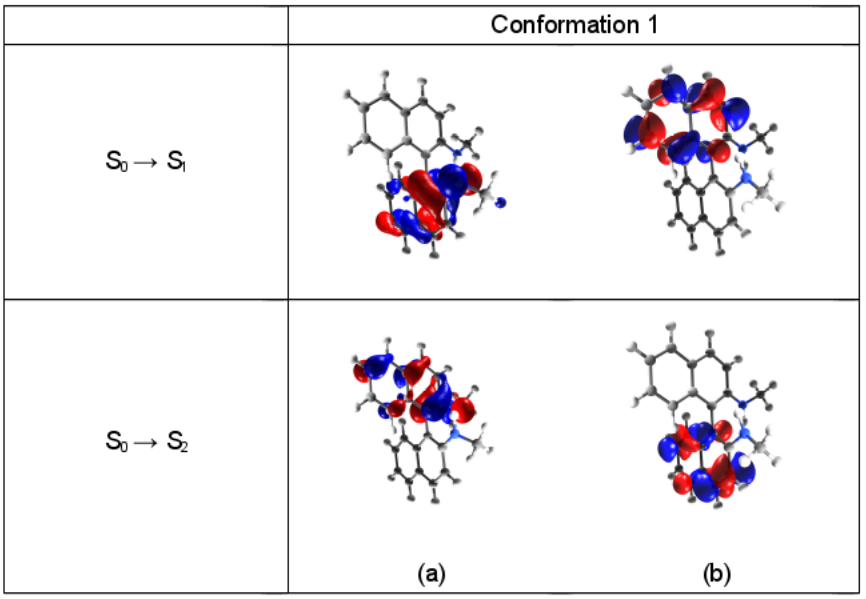


FIGURE 5.16: Most dominant occupied (a) and virtual (b) natural transition orbitals of (S)-DMBDA for the transition from ground state to first and second excited state as visualized on the ground state (S_0) structure

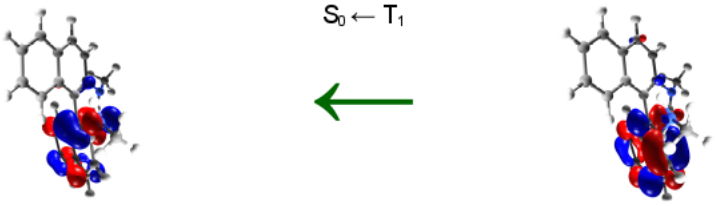


FIGURE 5.17: The natural transition orbitals for the spin-forbidden triplet-singlet transitions corresponding to circularly-polarized phosphorescence in S-DMBDA

TABLE 5.12: Rotational strengths [*esu cm erg* G^{-1}] and energies ΔE (eV) of different transitions in S-DMBDA

Transition	Rotational Strength	Energy
$S_0 \rightarrow S_1$	2.81×10^{-39}	3.67
$S_0 \rightarrow S_2$	-5.62×10^{-39}	3.73
$S_1 \rightarrow S_0$	5.85×10^{-39}	2.87
$T_1 \rightarrow S_0$	5.96×10^{-47}	2.23

Chapter 6

Summary

In summary, dipole and rotational strengths of circular dichroism, circularly polarized fluorescence and phosphorescence were calculated for β, γ - enones and ketones with conjugated double bonds using wave function based method RI-CC2. Calculation of CD and CPF is trivial because singlet-singlet transitions are spin-allowed in nonrelativistic quantum mechanics. However, for spin-forbidden CPP spin-orbit coupling with perturbation theory was employed within a response theory framework. For closed-shell molecules containing only light elements, a spin-free formalism was used to treat the singlet-triplet transitions [19].

A test molecule, Hydrogen Peroxide, was used to establish gauge-origin invariance in velocity gauge formulation and to check for basis set dependency. Aug-cc-pVDZ basis set was found to provide sufficient accuracy for the calculations of transition strengths. A two-component relativistic calculation was also performed for comparison. The oscillator strengths and rotator strengths from the nonrelativistic calculations compared well with X2C-CC2 results.

The β, γ - enones and conjugated ketones gave CD, CPF and CPP strengths which compared well with that of DFT calculations. The β, γ - enones exhibit two minima with similar energies (≈ 0.05 eV) in the first excited singlet and triplet state. In some cases, the RI-CC2 calculations predict opposite signs for rotator strengths for the two minima which is related to the puckering of carbonyl group in the excited state with respect to the C=C double bond. However, the conjugated diketones with single minimum in the excited states also exhibited opposite signs for CPL with respect to CD in some low-lying

excited states without the puckering of carbonyl group.The CPP rotational strengths are four orders of magnitude smaller than that of corresponding CPF rotational strengths.

SOC-PT-CC2 which utilizes the RI approximation is applicable for larger molecules. In this master project, the rotational strength for spin-forbidden circularly-polarized phosphorescence was calculated for a mid-sized metal-free chiral aromatic system, S-DMBDA, containing 44 atoms.

Appendix A

Conversion factors

Dipole strengths and rotational strengths were converted from atomic units to CGS units for comparison of results with the references [11, 16] which is based on reference [48].

1 au of dipole strength $(e^2 a_o^2) = 6.460\,48 \times 10^{-36} esu^2\ cm^2$
1 au of rotational strength $\left(\frac{e^2 \hbar^2 a_o}{m_e}\right) = 4.714\,44 \times 10^{-38} esu\ cm\ erg\ G^{-1}$

Appendix B

Wigner-Eckart Theorem

Consider the WET[31],

$$\langle j'm'''|T^{kq'}|jm''\rangle = (-1)^{m'''-m'} \frac{\begin{pmatrix} j' & k & j \\ -m''' & q' & m'' \end{pmatrix}}{\begin{pmatrix} j' & k & j \\ -m' & q & m \end{pmatrix}} \langle j'm'|T^{kq}|jm\rangle \tag{B.1}$$

In our case, $j' = 0$, $m''' = m' = 0$, $k = j = 1$. We need the $3j$ symbols $M = \begin{pmatrix} 0 & 1 & 1 \\ 0 & q & m \end{pmatrix}$. The values are 0 for $q \neq -m$, so that $3j$ symbols $M = \begin{pmatrix} 0 & 1 & 1 \\ 0 & -m & m \end{pmatrix}$ are left which are $\frac{1}{\sqrt{3}}$ for $m = -1, +1$ and $\frac{-1}{\sqrt{3}}$ for $m = 0$.

Alternative method The equalities can also be evaluated for the current case using the definitions of the annihilation and the creation operators from second quantization.

Assume a triplet configuration state function with the three normalized components:

$$|ia; 1, +1\rangle = |1_{i\alpha}0_{i\beta}1_{a\alpha}0_{a\beta}\rangle \tag{B.2}$$

$$|ia; 1, 0\rangle = \frac{1}{\sqrt{2}}(|0_{i\alpha}1_{i\beta}1_{a\alpha}0_{a\beta}\rangle + |1_{i\alpha}0_{i\beta}0_{a\alpha}1_{a\beta}\rangle) \tag{B.3}$$

$$|ia; 1, -1\rangle = |0_{i\alpha}1_{i\beta}0_{a\alpha}1_{a\beta}\rangle \tag{B.4}$$

These components are related by a single excitation to a reference determinant $|ref\rangle = |1_{i\alpha}1_{i\beta}0_{a\alpha}0_{a\beta}\rangle$. The transition matrix elements with the spin tensor operators are as follows:

$$\begin{aligned}
\langle ref|\widehat{T}^{1,-1}_{ia}|ia;1,+1\rangle &= \langle 1_{i\alpha}1_{i\beta}0_{a\alpha}0_{a\beta}|a^{\dagger}_{i\beta}a_{a\alpha}|1_{i\alpha}0_{i\beta}1_{a\alpha}0_{a\beta}\rangle \\
&= \langle 1_{i\alpha}1_{i\beta}0_{a\alpha}0_{a\beta}|1_{i\alpha}0_{i\beta}1_{a\alpha}0_{a\beta}\rangle = +1 \qquad \text{(B.5)} \\
\langle ref|\widehat{T}^{1,0}_{ia}|ia;1,0\rangle &= \langle 1_{i\alpha}1_{i\beta}0_{a\alpha}0_{a\beta}|a^{\dagger}_{i\alpha}a_{a\alpha} - a^{\dagger}_{i\beta}a_{a\beta}|\frac{1}{\sqrt{2}}(|0_{i\alpha}1_{i\beta}1_{a\alpha}0_{a\beta}\rangle + |1_{i\alpha}0_{i\beta}0_{a\alpha}1_{a\beta}\rangle) \\
&= \langle 1_{i\alpha}1_{i\beta}0_{a\alpha}0_{a\beta}|\frac{1}{\sqrt{2}}(-1+0+0-1)\frac{1}{\sqrt{2}}|1_{i\alpha}1_{i\beta}0_{a\alpha}0_{a\beta}\rangle = -1 \qquad \text{(B.6)} \\
\langle ref|\widehat{T}^{1,+1}_{ia}|ia;1,-1\rangle &= \langle 1_{i\alpha}1_{i\beta}0_{a\alpha}0_{a\beta}| - a^{\dagger}_{i\alpha}a_{a\beta}|0_{i\alpha}1_{i\beta}0_{a\alpha}1_{a\beta}\rangle \\
&= \langle 1_{i\alpha}1_{i\beta}0_{a\alpha}0_{a\beta}|1_{i\alpha}0_{i\beta}1_{a\alpha}0_{a\beta}\rangle = +1 \qquad \text{(B.7)}
\end{aligned}$$

Bibliography

[1] O. Christiansen, P. Jørgensen and C. Hättig, *International journal of quantum chemistry*, 1998, **68**, 1–52.

[2] O. Christiansen, J. Gauss and B. Schimmelpfennig, *Phys. Chem. Chem. Phys.*, 2000, **2**, 965–971.

[3] O. Christiansen and K. V. Mikkelsen, *The Journal of Chemical Physics*, 1999, **110**, 8348–8360.

[4] J. Hummelen, H. Wynberg, E. Meijer and H. Dekkers, *Nature (London)*, 1980, **265**,.

[5] B. Samoilov, *Zhur. Eksptl. i Teoret. Fiz.*, 1948, **Vol: 18**,.

[6] B. Pritchard and J. Autschbach, *ChemPhysChem*, 2010, **11**, 2409–2415.

[7] J. Schlessinger and A. Warshel, *Chemical Physics Letters*, 1974, **28**, 380 – 383.

[8] E. Anslyn and D. Dougherty, *Modern Physical Organic Chemistry*, University Science Books, 2006.

[9] C. Emeis and L. Oosterhoff, *Chemical Physics Letters*, 1967, **1**, 129 – 132.

[10] F. S. Richardson and J. P. Riehl, *Chemical Reviews*, 1977, **77**, 773–792.

[11] M. Pecul and K. Ruud, *Phys. Chem. Chem. Phys.*, 2011, **13**, 643–650.

[12] K. L. Bak, A. E. Hansen, K. Ruud, T. Helgaker, J. Olsen and P. Jørgensen, *Theoretica chimica acta*, 1995, **90**, 441–458.

[13] T. B. Pedersen, H. Koch and K. Ruud, *The Journal of Chemical Physics*, 1999, **110**, 2883–2892.

[14] C. Hättig, in *Response Theory and Molecular Properties (A Tribute to Jan Linderberg and Poul Jørgensen)*, ed. H. Jensen, Academic Press, 2005, vol. 50, pp. 37 – 60.

[15] C. Hättig and F. Weigend, *The Journal of Chemical Physics*, 2000, **113**, 5154–5161.

[16] M. Kaminski, J. Cukras, M. Pecul, A. Rizzo and S. Coriani, *Phys. Chem. Chem. Phys.*, 2015, **17**, 19079–19086.

[17] G. Longhi, E. Castiglioni, J. Koshoubu, G. Mazzeo and S. Abbate, *Chirality*, 2016, **28**, 696–707.

[18] W. Kutzelnigg and W. Liu, *The Journal of Chemical Physics*, 2005, **123**, 241102.

[19] B. Helmich-Paris, C. Hättig and C. van Wüllen, *Journal of Chemical Theory and Computation*, 2016, **12**, 1892–1904.

[20] O. Vahtras, H. Agren, P. Jørgensen, H. J. A. Jensen, T. Helgaker and J. Olsen, *The Journal of Chemical Physics*, 1992, **97**, 9178–9187.

[21] C. Hättig and F. Weigend, *The Journal of Chemical Physics*, 2000, **113**, 5154–5161.

[22] S. Hirata and M. Vacha, *The Journal of Physical Chemistry Letters*, 2016, **7**, 1539–1545.

[23] D. Caldwell and H. Eyring, *The Theory of Optical Activity*, Wiley-Interscience, 1971.

[24] J. Olsen and P. Jørgensen, *The Journal of Chemical Physics*, 1985, **82**, 3235–3264.

[25] T. Helgaker, P. Jørgensen and J. Olsen, in *Coupled-Cluster Theory*, John Wiley & Sons, Ltd, 2000, pp. 648–723.

[26] T. B. Pedersen and H. Koch, *The Journal of Chemical Physics*, 1997, **106**, 8059–8072.

[27] T. B. Pedersen and A. E. Hansen, *Chemical Physics Letters*, 1995, **246**, 1–8.

[28] K. Hald, C. Hättig and P. Jørgensen, *The Journal of Chemical Physics*, 2000, **113**, 7765–7772.

[29] T. Helgaker, P. Jørgensen and J. Olsen, in *Calibration of the Electronic-Structure Models*, John Wiley & Sons, Ltd, 2000, pp. 817–883.

[30] T. Helgaker, P. Jørgensen and J. Olsen, in *Spin in Second Quantization*, John Wiley & Sons, Ltd, 2000, pp. 34–79.

[31] C. M. Marian, in *Spin-Orbit Coupling in Molecules*, John Wiley & Sons, Inc., 2001, pp. 99–204.

[32] T. H. D. Jr., *The Journal of Chemical Physics*, 1989, **90**, 1007–1023.

[33] R. A. Kendall, T. H. D. Jr. and R. J. Harrison, *The Journal of Chemical Physics*, 1992, **96**, 6796–6806.

[34] M. Häser and R. Ahlrichs, *Journal of Computational Chemistry*, 1989, **10**, 104–111.

[35] G. Schaftenaar and J. Noordik, *Journal of Computer-Aided Molecular Design*, 2000, **14**, 123–134.

[36] C. Steffen, K. Thomas, U. Huniar, A. Hellweg, O. Rubner and A. Schroer, *Journal of Computational Chemistry*, 2010, **31**, 2967–2970.

[37] C. Lee, W. Yang and R. G. Parr, *Phys. Rev. B*, 1988, **37**, 785–789.

[38] S. Grimme, *Journal of Computational Chemistry*, 2006, **27**, 1787–1799.

[39] *TURBOMOLE, development version, 2015; For further information see* `http://www.turbomole.com`.

[40] *TURBOMOLE V7.1 2015, a development of University of Karlsruhe and Forschungszentrum Karlsruhe GmbH, 1989-2007, TURBOMOLE GmbH, since 2007; available from* `http://www.turbomole.com`.

[41] D. Peng, N. Middendorf, F. Weigend and M. Reiher, *The Journal of Chemical Physics*, 2013, **138**, 184105.

[42] K. Eichkorn, O. Treutler, H. Öhm, M. Häser and R. Ahlrichs, *Chemical Physics Letters*, 1995, **240**, 283 – 290.

[43] K. Krause and W. Klopper, *The Journal of Chemical Physics*, 2015, **142**, 104109.

[44] F. Weigend, A. Köhn and C. Hättig, *The Journal of Chemical Physics*, 2002, **116**, 3175–3183.

[45] F. Weigend, *Journal of Computational Chemistry*, 2008, **29**, 167–175.

[46] J. G. Hill and G. Bucher, *The Journal of Physical Chemistry A*, 2014, **118**, 2332–2343.

[47] R. L. Martin, *The Journal of Chemical Physics*, 2003, **118**, 4775–4777.

[48] P. J. Mohr, D. B. Newell and B. N. Taylor, *Journal of Physical and Chemical Reference Data*, 2016, **45**, 043102.